Equilibrium sediment exchange in the earth's critical zone: evidence from sediment fingerprinting with stable isotopes and watershed modeling

David Tyler Mahoney, Nabil Al Aamery, James Forrest Fox, Brenden Riddle, William Ford & Y. T. Wang

ONLINE FIRST

Journal of
Soils and Sediments
Assessment, Protection and Remediation
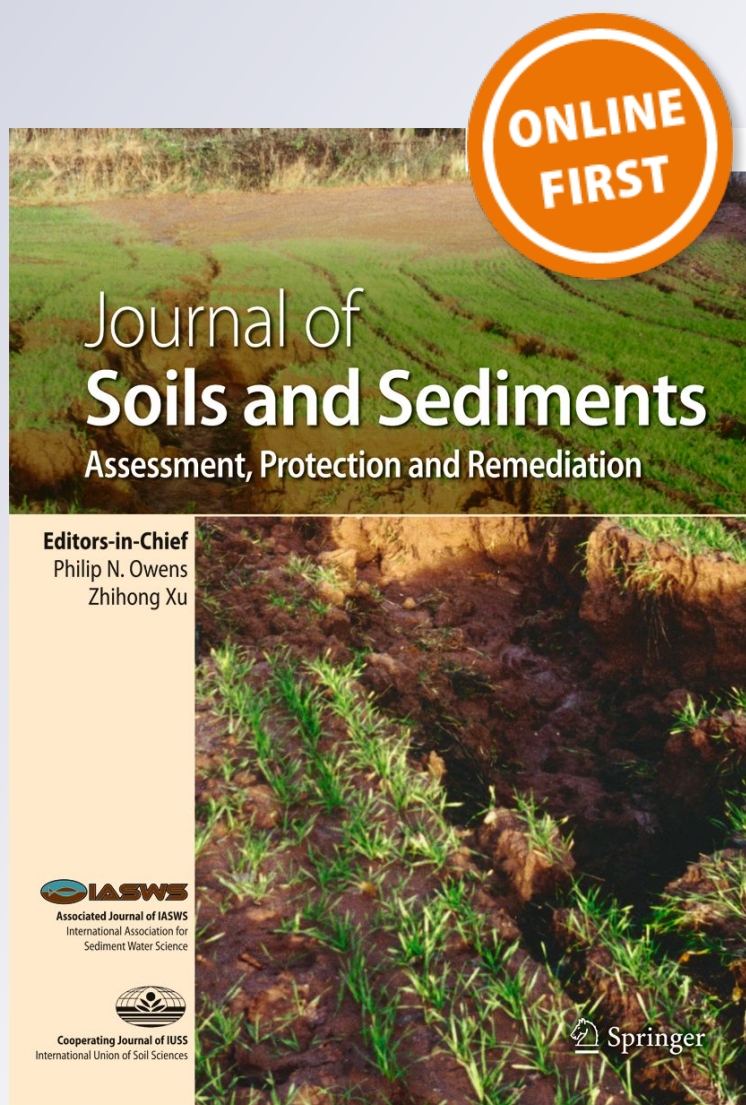
Editors-in-Chief
Philip N. Owens
Zhihong Xu

IASWS
Associated Journal of IASWS
International Association for
Sediment Water Science

Cooperating Journal of IUSS
International Union of Soil Sciences

⚘ Springer

⚘ Springer

Springer

CrossMark

Equilibrium sediment exchange in the earth's critical zone: evidence from sediment fingerprinting with stable isotopes and watershed modeling

David Tyler Mahoney [1] · Nabil Al Aamery [1] · James Forrest Fox [1] · Brenden Riddle [1] · William Ford [2] · Y. T. Wang [1]

© Springer-Verlag GmbH Germany, part of Springer Nature 2018

Abstract

Purpose The equilibrium sediment exchange process is defined as instantaneous deposition of suspended sediment to the streambed countered by equal erosion of sediment from the streambed. Equilibrium exchange has rarely been included in sediment transport studies but is needed when the sediment continuum is used to investigate the earth's critical zone.

Materials and methods Numerical modeling in the watershed uplands and stream corridor simulates sediment yield and sediment source partitioning for the Upper South Elkhorn watershed in Kentucky, USA. We simulate equilibrium exchange when upland-derived sediment simultaneously deposits to the streambed while streambed sediments erode. Sediment fingerprinting with stable carbon isotopes allowed constraint of the process in a gently rolling watershed.

Results and discussion Carbon isotopes work well to partition upland sediment versus streambed sediment because sediment deposited in the streambed accrues a unique autotrophic, i.e., algal, fingerprint. Stable nitrogen isotopes do not work well to partition the sources in this study because the nitrogen isotope fingerprint of algae falls in the middle of the nitrogen isotope fingerprint of upland sediment. The source of sediment depends on flow intensity for the gently rolling watershed. Streambed sediments dominate the fluvial load for low and moderate events, while upland sediments become increasingly important during high flows and extreme events. We used sediment fingerprinting results to calibrate the equilibrium sediment exchange rate in the watershed sediment transport model.

Conclusions Our sediment fingerprinting and modeling evidence suggest equilibrium sediment exchange is a substantial process occurring in the system studied. The process does not change the sediment load or streambed sediment storage but does impact the quality of sediment residing in the streambed. Therefore, we suggest equilibrium sediment exchange should be considered when the sediment continuum is used to investigate the critical zone. We conclude the paper by outlining future research priorities for coupling sediment fingerprinting with watershed modeling.

Keywords Carbon stable isotopes · Sediment continuum · Sediment fingerprinting · Watershed sediment transport modeling

✉ James Forrest Fox
james.fox@uky.edu

1 Department of Civil Engineering, University of Kentucky, 354G O. H. Raymond Bldg., Lexington, KY 40506-0281, USA

2 Department of Biosystems & Agricultural Engineering, University of Kentucky, Lexington, KY, USA

1 Introduction

A deep understanding of sediment continuum dynamics provides a valuable framework in which to evaluate the streambed as part of the critical zone's response to human impacts. Scientists are now well aware that the sediment continuum in a stream and watershed system is more akin to discontinuities in sediment mobilization and sustained transport than continuity or linearity (e.g., Phillips 2003; Fryirs 2013). The current sediment paradigm is best framed by considering a range of morphologic features across both the landscape surface and stream corridor that are connected or disconnected as a function of nonhydrologic and hydrologic thresholds (e.g., Bracken

Springer

Table 1 Review of organic tracers applied in sediment fingerprinting studies

Study	Watershed (km²)	Sediment sources	Organic tracers
Studies considering distal/upland sources with different land uses and vegetative cover			
Papanicolaou et al. (2003)	600	Winter wheat agriculture and conifer forest silt loam soil	δ^{13}C, δ^{15}N, C/N
Bellanger et al. (2004)	25**	Experimental coffee, maize, and bare plots	δ^{13}C, δ^{15}N, TOC, TN, C/N
Minella et al. (2004)*	1.3, 0.57	Cultivated areas, pastures, unpaved roads	TOC, TN, TP
Dalzell et al. (2007)	850	Corn, soybean, tall fescue	δ^{13}C, DOC
Gibbs (2008)*	117	Pastures, forested areas	δ^{13}C
Jacinthe et al. (2009)	Unspecified	Corn, soy bean, rye rotation, plowed continuous corn, no-till continuous corn	δ^{13}C
Kouhpeima et al. (2010)*	1.0, 5.4	Gullies, surface materials from various soil formations	TOC, TON, TOP
Nazari Samani et al. (2011)*	Unspecified	Gully side wall, dry farming and rangeland	OC, N, C/N
Studies considering distal/upland sources as well as streambanks or floodplains			
Walling et al. (1993)	46	Pastures, cultivated agriculture Streambanks	TOC, TN
Walling and Woodward (1995)*	276	Cultivated areas, pastures Streambanks	TOC, TON, TOP
Collins et al. (1997)*	46, 8.7	Pastures, cultivated areas, woodland Streambanks	TOC, TON, TOP
Walling et al. (1999)*	3315	Woodland topsoil, uncultivated topsoil, cultivated topsoil Streambanks	TOC, TON, TOP
Russell et al. (2001)*	2 (~4 km²)	Field drains, pastures, arable land, hopyards Streambanks	TOC, TN, TP
Walling et al. (2001)*	63	Cultivated areas, bush grazing, gullies Streambanks	TOC, TON
Gomez et al. (2003)	1580	Weathered bedrock from gullies, soil and regolith on hillslopes Floodplains	δ^{13}C, C/N
Walling (2005) (via Nicholls 2001; unpublished dissertation)*	258	Woodland topsoil, pastures, cultivated topsoil Streambanks	TOC, TON
Fox and Papanicolaou (2007)	0.71	Agricultural hillslopes Floodplains	δ^{13}C, δ^{15}N, C/N
Fox and Papanicolaou (2008a)	15	Logging in conifer forest, hay pastures, winter wheat and peas agriculture Winter wheat-floodplains	δ^{15}N, C/N
Fox and Papanicolaou (2008b)	600	Winter wheat-uplands, hay pastures, conifer forest, agricultural conservation reserve-uplands Winter wheat-floodplains, agricultural conservation reserve-floodplains	TOC, TON, TOP, δ^{15}N
Rhoton et al. (2008)*	150	Fan remnants, hillslopes, mountain slopes, alluvial fans Floodplains	δ^{13}C, δ^{15}N, C/N, TOC, TN
Fox (2009)	4 (~2 km²)	Surface coal mining, forested areas, reclaimed grassland, geogenic organic matter Streambanks	δ^{13}C, δ^{15}N, TOC, TN
Gellis et al. (2009)*	109–156	Construction sites, ditches, agricultural topsoil, forested areas Streambanks and floodplains	δ^{13}C, δ^{15}N, TOC, TN
Mukundan et al. (2010)*	182	Croplands, pastures, forested areas, unpaved roads, construction sites Streambanks and floodplains	δ^{15}N
Mukundan et al. 2011*	182	Croplands, pastures, forested areas, unpaved roads, construction sites Streambanks	TOC, TN
Blake et al. (2012)*	1.45	Maize agriculture, winter wheat agriculture, pastures, wooded areas Streambanks	δ^{13}C
Jung et al. (2012)	60	Forested areas, cultivated fieldsStreambanks	δ^{13}C, δ^{15}N, TOC
Hancock and Revill (2013)*	3860	Cultivated areas, forested areas, pastures, subsoils Streambanks	δ^{13}C
Slimane et al. (2013)*	2.63	Cropland topsoils, grasslands, scrublands, gullies Streambanks	TOC, TN
Fox and Martin (2015)	3.5, 2.2	Surface reclaimed mining soils, forested areas Streambanks	δ^{13}C, δ^{15}N, TOC, TN
Smith and Blake (2014)*	920	Pastures, cultivated topsoil	TOC

Table 1 (continued)

Study	Watershed (km^2)	Sediment sources	Organic tracers
Laceby et al. (2015)	75, 123, 311	Streambanks	δ^{13}C, δ^{15}N, TOC, TN, C/N
		Gullies, cultivated agriculture, grazing pastures, natural grazing land	
Stewart et al. (2015)*	324	Streambanks	δ^{13}C, δ^{15}N, TOC, TN
		Forested areas, roads, pastures, cropland topsoil	
Laceby et al. (2016)	171, 265, 77	Streambanks	δ^{13}C, δ^{15}N, TOC, TN
		Cultivated topsoil, forested areas, subsoils	
McCarney-Castle et al. (2017)	217	Upland surfaces	δ^{13}C, δ^{15}N
		Streambanks	
Studies considering streambed and other sources			
McConnachie and Petticrew (2006)	75	Organic matter sources	δ^{13}C, δ^{15}N, C/N
		Leaf litter, detritus	
		Algae, periphyton, decaying salmon	
Bonn and Rounds (2010)	1840	Leaf litter, upland soils, detritus	δ^{13}C, δ^{15}N, C/N
		Suspended sediment, macrophytes, phytoplankton, periphyton, wastewater treatment effluent	
Fox et al. (2010)	61.8	Streambanks, bank slumping	δ^{15}N, TOC, TN, C/N
		Streambed	
Schindler Wildhaber et al. (2012)	31	Forested areas, pastures, arable land	δ^{13}C, δ^{15}N, C/N
		Riverbed, algae	
Cooper et al. (2015)*	5.4	Organic matter sources	δ^{13}C
		Streambed sediments	
McCorkle et al. (2016)	Unspecified	Surface erosion (O horizon)	δ^{13}C, δ^{15}N, C/N
		Streambanks	
		Streambed	
Rose et al. (2018)*	7.25	Agricultural surface soil, forested surface and subsurface soil, pastures, gullies	OC, ON, C/N δ^{13}C, δ^{15}N
		Streambanks	
		Floodplains	
		Streambed	
Zhang et al. (2017)*	3 (~70 km^2)	Farmyard manures/slurries, damaged road verges, septic tanks	δ^{13}C, δ^{15}N
		Decaying instream vegetation, watercress farms, fish farms	

*Note: These studies also applied inorganic and/or radionuclide tracers. Only organic tracers are tabulated herein

**30 m^2 plots within the 25-km^2 catchment

et al. 2015). We suggest more emphasis on the streambed and a process termed "equilibrium sediment exchange" should be considered when the critical zone is evaluated with the sediment continuum. Equilibrium sediment exchange is the process of instantaneous deposition of upland-derived suspended sediment to the streambed countered by equal erosion of instream sediment from the streambed (Husic et al. 2017). The process does not change the suspended sediment load or the stored mass of sediment in the streambed reflecting equilibrium sediment continuity (e.g., Chang 1988). Equilibrium sediment exchange occurs because low momentum zones of sweeping coherent fluid episodically deposit sediment to the streambed while fluid ejections episodically resuspend bed sediment to the water column (Cellino and Lemmin 2004; Husic et al. 2017). The equilibrium sediment exchange process of simultaneous deposition and erosion is known to exist

(Cellino and Lemmin 2004; Winterwerp and Van Kesteren 2004) but is rarely included in fluvial sediment transport models (Husic et al. 2017).

Sediment fingerprinting using organic tracers provides a potential tool to estimate the contribution of sediment from upland-derived and instream-derived streambed sediment and, in turn, assist with parameterizing equilibrium sediment exchange during watershed sediment transport modeling. Our literature review (see Table 1) suggests few studies have used sediment fingerprinting with organic tracers to partition upland-derived versus streambed-derived sediments, albeit we recognize several studies have considered the streambed source. Organic tracers are expected to partition upland and streambed sediments for the scenario when upland sediment deposits to the streambed and then accrues a unique fingerprint from the autotrophy of the streambed. Therefore, the success

of the approach will be conditional on a biogeochemically active streambed, an accrued organic tracer signature that is unique, and the presence of instream fluvial storage in the streambed. Another consideration is the streambed may be continuously evolving due to physical and biogeochemical processes. Thus, we might expect the organic tracer fingerprint to be nonstationary (Fox et al. 2010; Ford et al., 2015a, b), which needs to be accounted for during critical zone simulation.

Sediment fingerprinting may partition upland and instream sediments; however, we realize that sediment fingerprinting alone cannot provide answers such as the time-varying nature of erosion and deposition rates, equilibrium sediment exchange rates, and continuous sediment flux from a watershed. Coupling sediment fingerprinting with watershed modeling provides a useful composite tool for estimating sediment process rates and serves as a potentially new class of sediment transport studies. In the present study, we couple sediment fingerprinting with an upland sediment transport model that estimates sediment connectivity in a spatially explicit manner (Mahoney et al. 2018) and an instream sediment transport model explicitly accounting for benthic sediment stores including both consolidated legacy sediments and the surficial fine-grained laminae (Russo and Fox 2012). We were motivated to investigate how sediment fingerprinting of upland and instream sediments could be useful for calibrating the equilibrium sediment exchange process.

The overall goal of this paper was to investigate equilibrium sediment exchange using sediment fingerprinting and watershed sediment transport modeling. Specific objectives were to (1) test and, if applicable, use sediment fingerprinting with stable carbon and nitrogen isotopes to partition upland sediment versus streambed sediment; (2) couple sediment fingerprinting with watershed sediment transport modeling and use sediment fingerprinting to calibrate the equilibrium sediment exchange process; and (3) investigate the role the equilibrium sediment exchange process plays when applying the sediment continuum to study the earth's critical zone.

2 Theoretical development

Figure 1 outlines the sediment transport processes in a gently rolling watershed framing the basis of our theoretical development. The upland morphology of gently rolling watersheds includes relatively stable land surfaces and ephemeral sediment pathways (e.g., swales, gullies, roadside ditches) (Jarritt and Lawrence 2007; Ford 2011; Ford and Fox 2014; Mahoney et al. 2018). Mild hillslopes and fertile soils support agricultural and urban/suburban land uses, which further stabilize upland sediment

pathways and floodplains (Mahoney et al. 2018). Low gradient to near-zero gradient microtopography of gently rolling landscapes can stifle sediment transport (Mahoney et al. 2018), and the floodplains can disconnect entire hillslopes from downstream sediment transport (Fryirs et al. 2007a, b; Mahoney et al. 2018). Sediment delivered from the uplands to the stream corridor during hydrologic events often fallout to temporarily stored streambed deposits because the sediment transport-carrying capacity cannot sustain the upland sediment inputs (Russo 2009).

In the stream network, streambed storage of fluvial sediment can include consolidated legacy sediments as well as a biologically active, unconsolidated layer known as the surficial fine-grained laminae (or SFGL, Droppo and Stone 1994; Droppo and Amos 2001). The agricultural land use of gently rolling systems produces dissolved nutrient loading to the stream that supports autotrophy, such as benthic algae growth in and above the SFGL (Ford and Fox 2017). The SFGL is a sediment layer on the order of a few millimeters to centimeter thick, is fluffy and neutrally buoyant with high water content, and has interparticle–interfloc pores where biological processes are persistent (Droppo and Stone 1994; Droppo and Amos 2001). The SFGL can accumulate organic matter, and the flora and fauna of the SFGL have been reviewed previously (see Russo and Fox 2012, and references therein) and include autotrophic algae, fungi, macrophytes, benthic macroinvertebrates (e.g., crayfish, aquatic worms), biofilm development via the live bodies of microorganisms and their excretions, and heterotrophic bacteria responsible for carbon turnover and nitrogen mineralization. Taken together, these biological processes of the SFGL have the potential to impact sediment transport through binding and decomposition mechanisms while at the same time provide a unique organic fingerprint for sediment fingerprinting analyses.

As mentioned in Section 1, we consider equilibrium sediment exchange between the water column and streambed. Equilibrium sediment exchange is the process of instantaneous deposition of suspended sediment to the streambed countered by equal erosion of sediment from the streambed (Husic et al. 2017). Past findings allowed us to adopt equilibrium sediment exchange driven by the turbulent bursting phenomena (Cellino and Lemmin 2004). The sweeping motions of turbulent bursts permit fine sediments to arrive near bed deposits, allowing deposition. The ejection motion resuspends bed sediments in the water column. The downwelling–upwelling motion of turbulent bursting provides a conceptual model for representing the sediment exchange process, even during equilibrium conditions where zero change of suspended load in the water column occurs. We consider the total mass of sediment transferred during equilibrium

Fig. 1 Gently rolling watershed configuration and conceptualization. "Gently rolling" reflects "undulating" landscape slopes (i.e., not steep) with the potential for steeper sections of complex hillslopes classified as "rolling" (USDA 2017, p. 44)
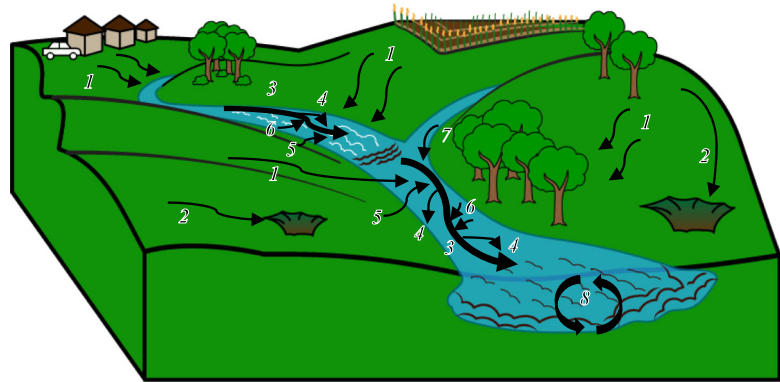
1 – Upland Erosion	*5 –Bank Erosion*
2 – Microtopography Deposition	*6 – SFGL and Bed Erosion*
3 – Instream Sediment Transport	*7 – Gully/Swale Sediment Transport*
4 – Deposition	*8 – Equilibrium Sediment Exchange*

exchange, S_x, as a function of sediment transport during bursting as follows:

$$S_x = \text{fn} \begin{bmatrix} \text{suspended sediment availability,} \\ \text{bed sediment availability, bursting, duration of the process} \end{bmatrix} \quad (1)$$

The components of Eq. (1) realize equilibrium exchange is not less simple than sediment transport prediction itself. Nevertheless, we may begin to substitute likely governing variables controlling the components of Eq. (1) as:

$$S_x = fn\left[\{\overline{\overline{C}}_s, V_w, z^*, d_{ss}, \sigma_{ss}\}, \{d_{ss}, \sigma_{ss}, d_{bs}, \sigma_{bs}, (\tau_{burst} - \tau_{cr})\}, \{S_B, T_B^{-1}, k_s, H\}, \{t_d\}\right] \quad (2)$$

The first group of variables reflects the availability of suspended sediment in the water column to exchange with the bed including the double-averaged suspended sediment concentration ($\overline{\overline{C}}_s$), the volume of water in the channel (V_w), the distribution of suspended sediment in the vertical via the Rouse number (z^*), and properties of the suspended sediment particle size distribution (d_{ss}, σ_{ss}). Bed sediment availability for exchange may be represented with a bed sediment supply threshold (d_{ss}, σ_{ss}), particle size distribution of the bed (d_{bs}, σ_{bs}), and excess shear to allow transport during bursting ($\tau_{burst} - \tau_{cr}$). Bursting action to cause exchange may reflect the energy of turbulent bursting (S_B), the time scale of bursting called the bursting period (T_B^{-1}), and the distribution of bursting in the water column as a function of the roughness height of the streambed (k_s) and the flow depth (H). Finally, the duration (t_d) of equilibrium exchange is included, which reflects that our interest is not in the exchange from a single burst but rather the cumulative impact on streambed and suspended sediment over some period (e.g., hour, hydrologic event, year).

Our theoretical development in Eqs. (1) and (2) does not provide a predictive model of equilibrium exchange but does provide variables for consideration in systems where it exists

and may vary through space and time. The gently rolling watershed is argued to provide such conditions given the high suspended sediment loads during hydrologic events, pronounced fluvial storage, and ubiquitous nature of turbulent bursting. As will be shown, we use sediment fingerprinting to empirically calibrate the equilibrium exchange process. We then consider the factors in Eqs. (1) and (2) in our discussion of governing processes in the basin. Sediment fingerprinting is useful in calibrating S_x because it partitions suspended sediment arriving from the uplands with streambed sediments.

3 Study site and materials

The study site was the gently rolling Upper South Elkhorn watershed in the Inner Bluegrass Region of Kentucky, USA (see Fig. 2). The Upper South Elkhorn watershed (61.8 km^2) fits in the "gently rolling" classification previously described due to generally low gradient hillslopes with interspersed "rolling" surfaces with increased slope (Sims et al. 1968; McGrain 1983). Bedrock outcrops located throughout the stream network control longitudinal stream morphology and
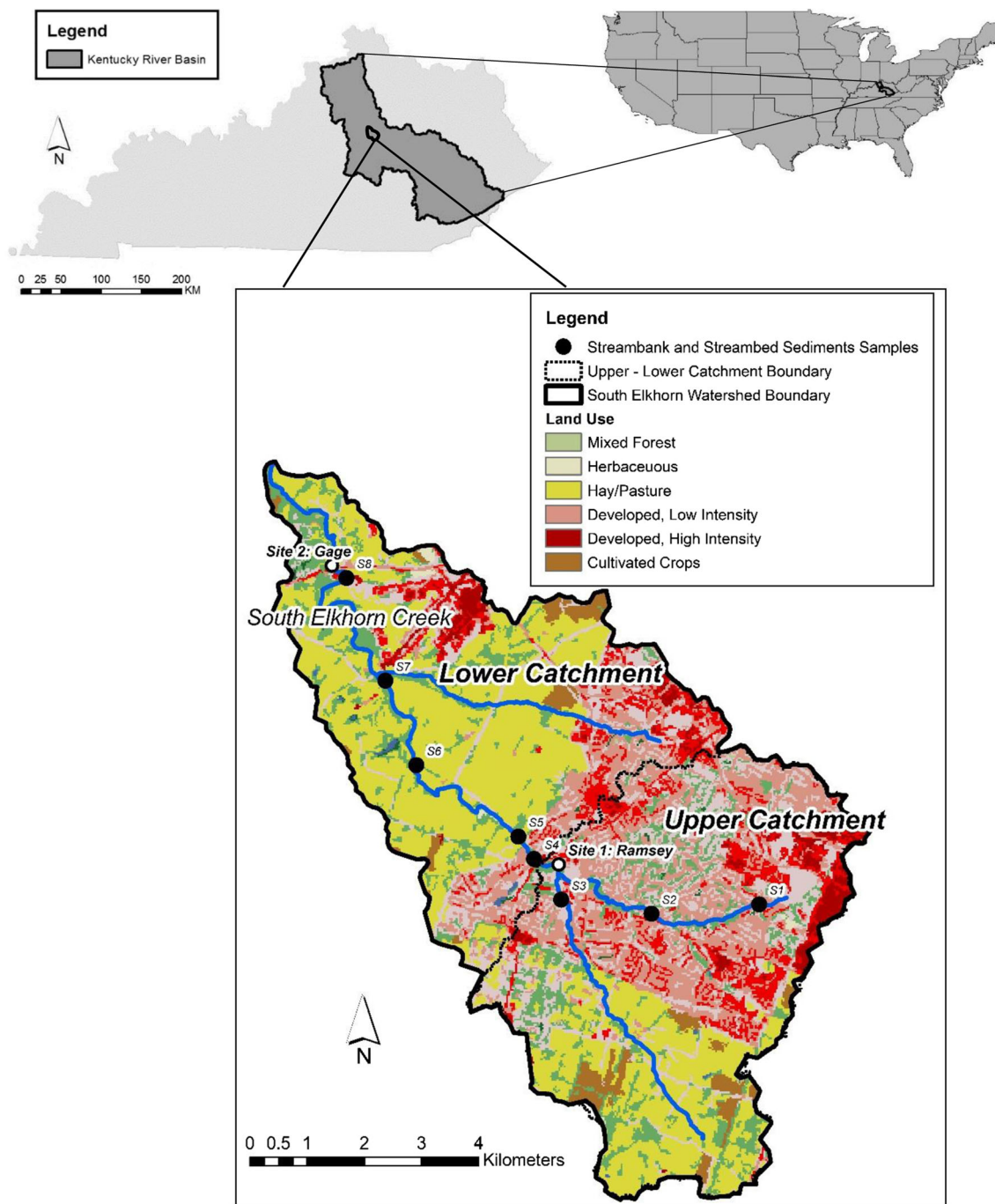
Fig. 2 Study watershed, land use, instream sample site locations (from Fox et al. 2010), and stream location within the Kentucky River Basin, USA. Land use in the upper catchment is primarily urban (60% urban, 40% agricultural). Land use in the lower catchment is primarily agricultural (72% agricultural, 28% urban). Samples of sediment sources from the stream corridor were collected in eight locations (labeled S1–S8) in the study watershed and defined the isotopic signature of instream sediments, banks sediments, and algae

create instream deposits of fine sediment. We selected this watershed to investigate the ability of sediment fingerprinting and modeling to elucidate equilibrium exchange because: (i) low gradient watersheds such as the Upper South Elkhorn foster life-sustaining ecosystem processes throughout earth's critical zone; (ii) anthropogenic disturbance to the critical zone is often pervasive in low gradient watersheds due to their

adeptness for sustaining life; (iii) scientists recognize the importance of low gradient watersheds in global nutrient and sediment budgets (e.g., Fox et al. 2010; Ford and Fox 2014); and (iv) we have extensive materials associated with historical and ongoing data collection conducted by the University of Kentucky, USGS, and Lexington-Fayette County Urban Government including raw and detrended data, information,

and resources published in our group's previous journal papers.

Materials used herein from previous assessments included establishing an upper and lower catchment and field assessment to gain background knowledge of the system (Mahoney 2017; Mahoney et al. 2018). Two different long-term sediment data collection sites have been established in South Elkhorn Creek (see Fig. 2), and the locations nearly divide the watershed in half. The upper catchment above site 1 is dominated by urban land uses (60% urban, 40% agricultural, Fox et al. 2010), and the lower catchment between site 1 and site 2 is primarily agricultural (28% urban, 72% agricultural, Fox et al. 2010). The entire Upper South Elkhorn watershed is predominantly agricultural land use (44% urban, 55% agricultural, Mahoney et al. 2018). Upland field reconnaissance has shown suburban grass lots and agricultural pastureland dominate upland land cover. Geospatial analyses of sediment connectivity in the uplands have shown upland sediments are primarily derived from gullies, swales, and roadside ditches (Mahoney et al. 2018). Instream field assessments have shown pronounced storage of fluvial sediment throughout South Elkhorn Creek, and estimated streambed storage exceeds the annual sediment yield (Russo 2009; Mahoney 2017; Mahoney et al. 2018).

Materials for this study also included a collection of published stable isotope data of soils, sediments, and algae. Nearly a decade of stable isotope measurements of transported sediments collected from sites 1 and 2 in Fig. 2 was published for the system (Ford 2014; Ford et al. 2015a). We collected the transported sediments approximately weekly using sediment traps (Phillips et al. 2000) and performed stable carbon and nitrogen isotope analyses and elemental analyses for all sediment after preprocessing and wet sieving to retain the less than 53-μm size fraction of sediments (Fox et al. 2010; Ford et al. 2015a). Ford et al. (2015a) performed time-series analyses of the data streams including removal of the biological-associated mean trends with empirical mode decomposition analyses. The decomposition analyses accounted for the non-stationary mean in the present study. Stable isotope results of sediment sources have also been published, including stable carbon and nitrogen isotope measurements of streambed sediments, algae, and of grassland and agricultural soils from different particle size classes (see Fig. 2 for instream sediment sample locations; Davis 2008; Campbell et al. 2009; Fox et al. 2010; Ford et al. 2015a). Multiple years of sediment particle size distribution results for the study stream were performed using microscopy of fluvial sediments and are shown in Fig. 3 (from Fox et al. 2014).

Materials also included previously published and calibrated numerical models established for upland sediment transport, instream transport, and streambed storage for the Upper South Elkhorn watershed. A sediment connectivity and upland erosion model simulates transport thresholds and rates,

respectively, for the Upper South Elkhorn (Mahoney et al. 2018). A sediment transport and streambed evolution model developed for the stream corridor considers upland sediment supply to the stream corridor, bank processes, surficial fine-grained laminae processes, and fate of deeper bed sediments (Russo and Fox 2012).

4 Methods

4.1 Sediment fingerprinting of upland sediment versus streambed sediment

We characterized sediment sources in the watershed as originating from the uplands or the temporarily stored streambed deposits. The rather coarse characterization lumps together several subsources, as we will discuss, but this characterization was needed to investigate the equilibrium exchange process. For the scale considered (32.8 and 61.8 km^2), the upland sediment source classification lumps together all sediment classified as "not bed sediments" including surface soil from both agricultural and suburban/urban land uses as well as sediment eroded from subsurface soils of gully and swale pathways. Surface and subsurface soils eroded from streambanks are also included in the upland sediment classification, which is not necessarily typical. However, streambanks make up less than 1% of the sediment load in this watershed (Russo and Fox 2012). The temporarily stored streambed deposits lump together the SFGL at the surface of the streambed and deeper legacy sediments. However, in this system, the SFGL contribution dominates the instream sediment production due to its high supply and low critical shear stress (Russo and Fox 2012).

We apply stable carbon and nitrogen isotopes of sediment as potentially unique tracers for partitioning upland sediments versus streambed sediments. Stable carbon and nitrogen isotopes are reported using delta notation as $\delta^{13}C$ and $\delta^{15}N$ to
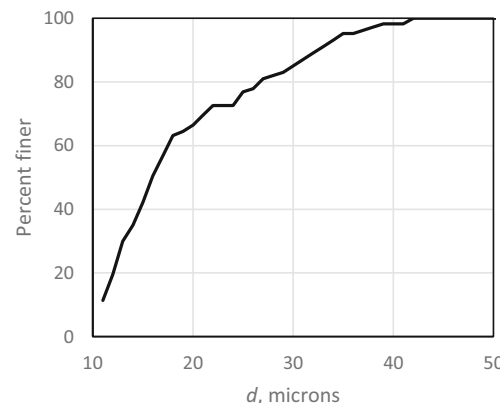

Fig. 3 Cumulative particle size distribution of fluvial sediments performed using microscopy in the Upper South Elkhorn watershed (see also data reported in Fox et al. 2014). *d* is the diameter of the particle in micrometers

indicate depletion (−) or enrichment (+) of the heavy (higher-mass) stable isotopes (^{13}C and ^{15}N) compared to the lighter mass stable isotopes (^{12}C and ^{14}N) and can be defined as

$$\delta X \ (\text{in‰}) = \left(\frac{R_{\text{sample}}}{R_{\text{std}}} - 1 \right) \times 10^3, \tag{3}$$

where R_{sample} is the isotope ratio (^{13}C/^{12}C or ^{15}N/^{14}N) of the sample and R_{std} is the isotope ratio of the standard (Vienna Pee Dee Belemnite, VPDB, and atmospheric nitrogen, respectively). Stable carbon and nitrogen isotope measurements of transported and source sediments were previously collected (Davis 2008; Campbell et al. 2009; Fox et al. 2010; Ford et al. 2015a), as mentioned in Section 3.

Representing δ^{13}C and δ^{15}N of the sediment sources and sinks in the fingerprinting method required proper selection of samples to construct the distributions (Davis and Fox 2009) and consideration of source stationarity (Fox et al. 2010). We represented the upland sediment source with δ^{13}C and δ^{15}N measurements of surface and subsurface soils (Campbell et al. 2009; Fox et al. 2010). We considered δ^{13}C and δ^{15}N of the less than 53-μm fraction of the soil since this was the sediment particle size class we investigated. We assume δ^{13}C and δ^{15}N of upland sediment were stationary. Fox (2006) found a lack of seasonal or annual change for the less than 53-μm size fraction of upland soil, which agrees with the relatively long turnover time of finer-sized, more recalcitrant organic matter fractions of the soil (Cambardella and Elliott 1992). While disturbances likely existed throughout the uplands, we feel an assumption of stationarity is reasonable given that grass cover and silt loam dominated the land cover and soils, respectively, in both agriculture and suburban regions. We represented the streambed sediment with δ^{13}C and δ^{15}N measurements of sediment collected via the Lambert and Walling (1988) method during low flow periods ($Q_{\text{pk2}} < 2.8 \ \text{m}^3 \ \text{s}^{-1}$, where Q_{pk2} is the peak water discharge at location two during the sediment collection period) when only instream sediment was transported. We verified this method by comparing low flow sample results with streambed sediments collected during the same period and found only 0.2‰ difference or less.

We assumed the streambed isotope values are nonstationary given mean trends found in the published isotope data of streambed and transported sediments (Davis 2008; Fox et al. 2010a; Ford et al. 2015a). We subtracted the mean trend using empirical mode decomposition to account for the nonstationarity (Ford et al. 2015a). After decomposition, δ^{13}C and δ^{15}N of transported sediment included 189 and 232 measurements at sites 1 and 2, respectively, collected over a range of low, moderate, and extreme hydrologic events. Based on flow dependence of the dataset and previous study of sediment transport in the watershed (Russo and Fox 2012; Mahoney et al. 2018), we divided the datasets in four flow

regimes including low flow events ($Q_{\text{pk2}} < 2.8 \ \text{m}^3 \ \text{s}^{-1}$), moderate events ($2.8 \ \text{m}^3 \ \text{s}^{-1} < Q_{\text{pk2}} < 12.2 \ \text{m}^3 \ \text{s}^{-1}$), high flow events ($12.2 \ \text{m}^3 \ \text{s}^{-1} < Q_{\text{pk2}} < 24.4 \ \text{m}^3 \ \text{s}^{-1}$), and extreme hydrologic events ($Q_{\text{pk2}} > 24.4 \ \text{m}^3 \ \text{s}^{-1}$). We adjusted these flow regimes by a factor of 0.53 from the lower catchment (presented above) to the upper catchment using the area weighted method. We performed source allocation via unmixing for each flow regime and individual hydrologic events corresponding to each sediment trap sample.

We estimated source allocation using an unmixing model analysis specific to δ^{13}C and δ^{15}N (Fox and Martin 2015). The δ^{13}C and δ^{15}N signatures of sediment indicate the fingerprint of "sediment carbon" and "sediment nitrogen," respectively, rather than the fingerprint of the total sediment. Therefore, the carbon and nitrogen concentration of sediment corrected the source allocation in the unmixing model. The elemental concentrations were measured with a coupled elemental analyzer during stable isotope ratio mass spectroscopy, which is a typical analytical setup in the laboratory, and therefore, the added data needs did not place an undue burden on the researcher. Our correction was analogous to organic matter and particle size corrections included in the traditional model of Collins et al. (1997) and widely cited thereafter, albeit only carbon and nitrogen concentration corrections were needed for unmixing with δ^{13}C and δ^{15}N because the concentration changes of soil are highly correlated with particle size shifts (e.g., Cambardella and Elliott 1992; Campbell et al. 2009). Fox and Martin (2015) extensively described the unmixing model formulation and only the primary governing formulae are included here. Unmixing simulation with δ^{13}C and δ^{15}N were performed as:

$$\delta^{13}C_{\text{T}} = \sum_{i=1}^{n} \alpha_i \delta^{13} C_i X_{\text{C},i}, \tag{4}$$

$$\delta^{15}N_{\text{T}} = \sum_{i=1}^{n} \beta_i \delta^{15} N_i X_{\text{C},i} \frac{\text{ER}_{\text{N},i}}{\text{ER}_{\text{C},i}} \frac{(^{\text{N}}/_{\text{C}})_i}{(^{\text{N}}/_{\text{C}})_{\text{T}}}, \text{ and} \tag{5}$$

$$P_i = \frac{X_{\text{C},i} \left(\dfrac{\text{TOC}_{\text{T}}}{\text{ER}_{\text{C},i}\text{TOC}_i} \right)}{\sum_{i=1}^{n} \left(X_{\text{C},i} \dfrac{\text{TOC}_{\text{T}}}{\text{ER}_{\text{C},i}\text{TOC}_i} \right)}, \tag{6}$$

where T and i indicate transported and source i, respectively; α and β indicate functions for nonconservative δ^{13}C and δ^{15}N during transport; ER_{N} and ER_{C} are the enrichment ratios; N/C is the nitrogen to carbon atomic ratio of sediment; X_{C} is the carbon mass fraction; and TOC is the organic carbon concentration of sediment. Equations (4), (5), and (6) were solved together with constraints of unity for summation of both sediment carbon fractions and summation of sediment fractions. We corrected for the shifts in sediment carbon and sediment nitrogen from the sediment sources to sinks using the above equations. We treat the nonconservative functions and

enrichment ratios as zero given the source to sink transport is less than 1-day transit time. We also performed a Monte Carlo robust analysis to account for uncertainty. Isotope tracer distributions were assumed normal and parameterized via data mean and variance estimates. Each realization of the Monte Carlo simulation was solved via a random number generator to draw from the tracer distributions. We performed a sensitivity analysis of the ensemble size, and we found 10^5 realizations produced stable results for the ensemble first- and second-order moments. Therefore, we used 10^5 realizations for each ensemble solved.

4.2 Numerical modeling of the equilibrium sediment exchange

Numerical modeling of the equilibrium sediment exchange required coupling an existing upland erosion model (Mahoney et al. 2018) with an existing instream sediment transport model (Russo and Fox 2012) and sediment fingerprinting. As outlined in Mahoney et al. (2018), we used sediment connectivity theory in conjunction with probability theory to model upland sediment transport pathways in the watershed (Borselli et al. 2008; Bracken et al. 2015). We predicted upland sediment delivery to the stream network by coupling the active contributing area predicted from the probability of connectivity model with a threshold-based erosion model. Next, the continuity equation modeled instream sediment transport from various upland and instream sediment sources (Russo and Fox 2012), and a new feature of the instream model was added herein to simulate equilibrium sediment exchange calibrated using sediment fingerprinting. The mentioned references described the original model formulations, and the model application is described briefly below. The new methods described here include inclusion of the equilibrium exchange process in the instream sediment continuity equation, refined calibration and global sensitivity analysis of the coupled model with both upland and instream components, and the calibration of the equilibrium exchange process using sediment fingerprinting.

The probability of connectivity model provided spatially explicit results for the sediment active contributing area in the watershed uplands. Ambroise (2004) defined the active contributing area as the portion of a catchment that actively transports sediment to the stream network at a particular time step. The model simulated connectivity at a given time step using hydrologic modeling results from the Soil and Water Assessment Tool (SWAT; see Al Aamery et al. (2016) for model validation), a high-resolution (2.5 m) DEM, soil critical shear stress, orthophotographs, and morphologic data collected from field reconnaissance and remote sensing (Mahoney et al. 2018). We used SWAT to model hydrologic scenarios given its ability to simulate the processes of overland runoff and subsurface antecedent moisture (Arnold et al. 1998;

Neitsch et al. 2011). The probability of sediment connectivity model represented the intersection of several threshold-based probability equations to simulate various upland sediment transport processes. Equations used to model the upland probability of sediment connectivity model have been included in the Electronic supplementary material I (see also Mahoney et al. 2018 for additional background). Simulation of the probability of connectivity model for the Upper South Elkhorn watershed took place using ArcMap (version 10.4) on a desktop PC (Intel® Core™ i7-6700 CPU at 3.40 GHz; 64-bit operating system, ×64-based processor) over the course of approximately 112 h for the 4-year simulation period.

We applied the upland erosion model to active contributing cells from the probability of connectivity model and simulated sediment flux from the uplands by integrating the volume of eroded upland sediment at a particular time step. Upland sediment flux was simulated as a function of the sediment erosion rate, as predicted by the Partheniades (1965) equation, the soil bulk density, and the bathymetry of the sediment transport pathways, as predicted by the probability of connectivity model. We allocated connected cells to the upper or lower catchment based on their geospatial location in the watershed, and the upland erosion model was individually applied to the discretized cells to determine the total upland sediment flux from the upper and lower catchment at a given time step. Equations used in the upland erosion model have been included in the section Electronic supplementary material I.

Inputs and parameter ranges used in the upland erosion model (see Table 2) included channel bathymetry, geospatial data, hydrologic data, sediment routing information, and soil properties. We specify several parameter ranges using literature-derived methods. Time of concentration surrogated the storm length when surface erosion occurred (Mahoney et al. 2018). Literature values defined soil parameter ranges for critical shear stress, relative roughness, and the erodibility coefficient (e.g., Alberts et al. 1995; Hanson and Simon 2001). We estimated sediment bulk density using Russo and Fox (2012). We empirically replicated the width of connected rills and ephemeral gullies using equations developed by Nachtergaele et al. (2002). Finally, we parameterized the longitudinal slope and contributing area of connected cells with geospatial analyses in ArcMap v 10.4. The channel length for the bins depended on the daily results from the probability of connectivity model.

The instream sediment model simulated sediment transport from five potential sources in the stream network by estimating erosion and deposition in a reach during a particular time step (Russo and Fox 2012). Sediment sources included the SFGL biofilm, SFGL sediment component, streambed, streambanks, and upland sediments. The model accounted for sediment erosion and deposition from each source and estimated the total contribution of each source to the total

sediment yield at a given time step. Erosion and deposition were functions of the transport capacity of the fluid, which we predicted using the stream's available energy to transport sediment (Julien and Simons 1985). The SFGL layer lies atop bed sediments and has a relatively lesser critical shear stress compared to bed sediments (Droppo and Stone 1994). Thus, we assumed the SFGL preferentially erodes before deeper bed sediments. Sediment flux predicted from the upland erosion model served as the supply of upland suspended sediment in the instream sediment transport model. To account for equilibrium erosion and deposition resultant of turbulent bursts and sweeps occurring simultaneously in a reach, we updated the sediment continuity equation of Russo and Fox (2012) herein to include the equilibrium sediment exchange process as:

$$SS_i^j = SS_{i-1}^j + \sum_{k=1}^{N} E_{i\,k}^j - D_i^j$$
$$+ \left(Q_{ss\ in_i}^j + Q_{ss\ up_i}^j - Q_{ss\ out_i}^j \right) * \Delta t, \tag{7}$$

$$S_{bed_i}^j = S_{bed_{i-1}}^j + D_{bed_i}^j - E_{bed_i}^j, \tag{8}$$

$$SS_{i+\frac{1}{2}}^j = SS_i^j - Exf * SS_i^j + Exf * S_{bed_i}^j * \left[\frac{SS_i^j}{S_{bed_i}^j} \right], \tag{9}$$

$$S_{bed_{i+\frac{1}{2}}}^j = S_{bed_i}^j - Exf * S_{bed_i}^j * \left[\frac{SS_i^j}{S_{bed_i}^j} \right] + Exf * SS_i^j, \tag{10}$$

where Exf is the sediment exchange factor, (j) represents the stream-reach, (i) represents the time step, (k) represents the sediment source, N represents the number of sediment sources, SS is the mass of sediment (kg), E is erosion (kg), D is deposition (kg), $Q_{ss\ in}$ is the sediment flow rate in the reach (kg s^{-1}), $Q_{ss\ up}$ is the sediment flow rate in the reach from the uplands (kg s^{-1}), $Q_{ss\ out}$ is the sediment flow rate out of the reach (kg s^{-1}), and S_{bed} is the mass of bed sediments (kg). Equations utilized in the instream sediment transport model have been included in Electronic supplementary material II. Electronic supplementary material III defines all parameters used in the modeling.

Table 3 shows the inputs and parameter ranges for the instream sediment transport model. We defined several initial ranges using literature values. Literature suggests the SFGL is neutrally buoyant and this is reflected by the SFGL density (Stone and Droppo 1994; Droppo and Amos 2001). The development time, maximum depth, and the generation rate of the SFGL biofilm and sediment were parameterized from Stone and Droppo (1994) and Droppo and Amos (2001). The ranges for the transport capacity coefficients were empirical and we optimized these during model calibration (Dou 1974; Ahmadi et al. 2006; Yan et al. 2008; Guy et al. 2009; Madej et al. 2009).

We determined the shear stress coefficient for unsteady flow by the boundary shear stress distribution for a trapezoidal channel (Chang 1988). Previous research assisted in parameterization of the critical shear stress coefficients and erodibility of the instream sediment sources (Droppo and Amos 2001; Hanson and Simon 2001; Sanford and Maa 2001; Simon and Thomas 2002). We estimated the mean settling velocity of suspended material based on particle size and shape for sediments in the Inner Bluegrass Region of Kentucky, USA, as described in Fox et al. (2014). The sediment routing and flood wave coefficients were based on the travel time between the two study points and flood routing theory (e.g., Gupta 2016). Field reconnaissance and remote sensing helped estimate the channel bathymetry. We parameterized the longitudinal channel slope with longitudinal profiles and GIS analyses of high-resolution (1.5 m) digital elevation models (KYAPED 2014).

Calibration and validation data included total suspended solids samples collected approximately every 2 h over the course of 32 storm events from 2007 until 2010 using a Teledyne ISCO automated sampler. Of the 32 sampled storm events, we deemed 18 storms suitable for use in calibration and validation based on the quality of the data. For example, we removed storms with little to no sediment transport from the calibration and validation process because they may bias evaluation statistics. Other qualitative calibration data included orthophotographs and visual reconnaissance of sediment transport pathways collected during field assessment.

Model evaluation consisted of a three-stage calibration and validation process and a global sensitivity and uncertainty analysis (Fig. 4). Stage 1 calibrated the upland probability of sediment connectivity model. Upon running the model, we visually compared simulated sediment transport pathways to known sediment transport pathways identified during field reconnaissance and from orthophotographs. If the predicted sediment transport pathways were unacceptable, then we iteratively adjusted parameters from the probability of connectivity model until calibration was acceptable.

Stage 2 calibrated the upland erosion and instream sediment transport models. We used 15 storms from 2007 to 2009 in model calibration and three storms in 2010 for model validation. Three objective functions evaluated the model's performance including: (1) the Nash Sutcliffe statistic of the simulated sediment flux and observed sediment flux for the 15 calibration storm events, (2) equilibrium of the streambed such that net aggradation and net degradation were nearly zero over the 4-year simulation period, and (3) long-term equilibrium of upland sediment flux and sediment flux from the watershed outlet. Sediment transport parameters in the upland erosion and instream sediment models were automatically adjusted

until each of the criteria was fulfilled. We included simulations fulfilling the three evaluation criteria with parameters in mutually permissible ranges based on the literature in the solution space. We performed quasirandom, low discrepancy Sobol sequencing to generate 10,000 sets of the 20 parameters in the coupled models. The 10,000 sets stabilized the results of the global sensitivity analysis and sediment yield. The global sensitivity analysis was

Fig. 4 Three-stage calibration procedure for stage 1 sediment connectivity model calibration, stage 2 upland erosion model and instream sediment model calibration, and stage 3 sediment source calibration
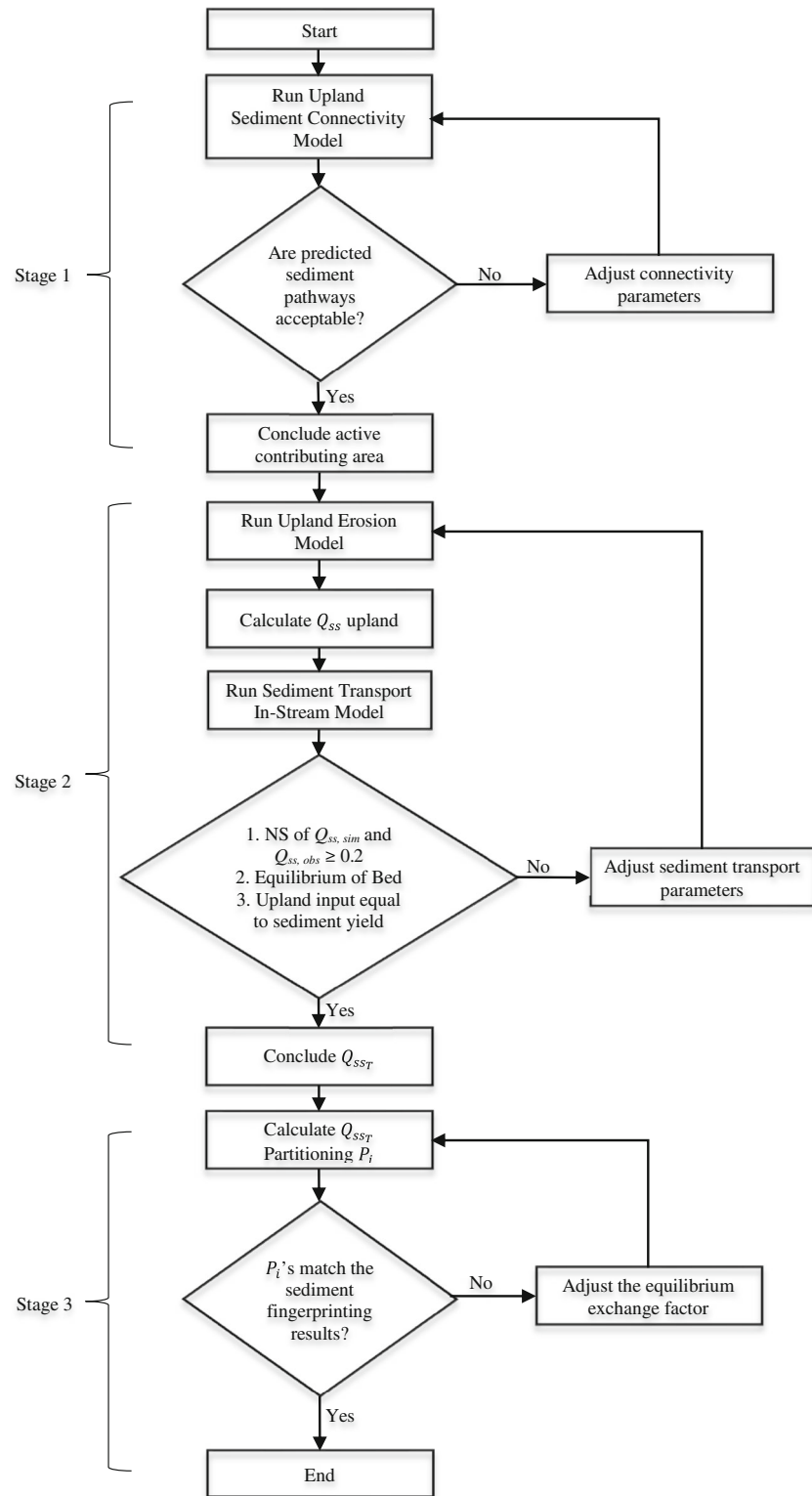
performed by determining the sensitivity indices (Joe and Kuo 2003; Saltelli et al. 2008).

Stage 3 calibrated the model's partitioning of sediment sources to the sediment fingerprinting results collected over the simulation period. We adjusted the equilibrium exchange factor shown in Eqs. (9) and (10) such that modeled sediment source partitioning from the sediment transport model matched the partitioned results from sediment fingerprinting. Four different exchange factors were used in both the upper catchment and lower catchment to represent adjustment of the equilibrium sediment exchange process across flow regimes.

5 Results and discussion

5.1 Sediment fingerprinting of upland sediment versus streambed sediment

We found $\delta^{13}C$ was able to discriminate the upland and instream sediment sources while $\delta^{15}N$ was unable to discriminate between the two sources. The $\delta^{13}C$ value of upland and instream sources was significantly different (p value < 0.001). The reason $\delta^{13}C$ worked well is because of the isotope signature differences for organic matter in the upland and instream sediments. Upland organic matter in this study site is from C3 plants, including northern grasses and to a lesser degree deciduous trees, with $\delta^{13}C$ from -27 to $-28‰$ (Campbell et al. 2009). During litter and root decomposition to soil carbon, isotopic enrichment of ^{13}C occurs for the more recalcitrant organic matter product (Nadelhoffer and Fry 1988). The $\delta^{13}C$ values of soils in the Bluegrass Region agree with the enrichment and show an increase in the value of $\delta^{13}C$ for surface soils, finer-sized sediment carbon pools, and with

depth in soil (Campbell et al. 2009). Subsurface soils show $\delta^{13}C$ values as low as $-23.9‰$ (Davis 2008). The streambed sediments acquire a $\delta^{13}C$ value that is distinct from the upland soil. Streambed sediments accrue stabilized benthic algae as the algae decompose (Ford and Fox 2017). $\delta^{13}C$ of algae is $-37.8(\pm 5.5)‰$ in South Elkhorn Creek (Ford et al. 2015a). Therefore, $\delta^{13}C$ of streambed sediment (temporal mean, $-27.3‰$) establishes a sediment fingerprint that is less than $\delta^{13}C$ of upland sediment (mean, $-25.9‰$).

We were unable to differentiate upland and instream sediment sources using $\delta^{15}N$ because the isotope distributions of upland and instream sediments were overlapping. The $\delta^{15}N$ value of the near-surface soil nitrogen with northern grasses is $2.5‰$ in this region (Campbell et al. 2009). During soil organic nitrogen mineralization, isotopic enrichment increases the $\delta^{15}N$ of the organic N substrate, and enrichment is on the order of two times that of carbon isotope enrichment (Nadelhoffer and Fry 1988). The isotope enrichment during mineralization is in agreement with data from our watershed and subsurface soils have $\delta^{15}N$ on average equal to $6.9‰$ (Davis 2008; Fox et al. 2010). Therefore, our upland sediment $\delta^{15}N$ value ranges from approximately 2 to 7‰. Similar to the carbon isotopes, streambed sediments accrue the $\delta^{15}N$ of autotrophs. $\delta^{15}N$ of algae is $4.95(\pm 1.6)‰$ in the South Elkhorn Creek (Ford et al. 2015a). $\delta^{15}N$ of algae falls in between the range of upland surface soil and upland subsurface soil. Therefore, the accrual of stabilized benthic algae in streambed sediments caused $\delta^{15}N$ to be an ineffective fingerprint for separating upland and streambed sediments.

The distribution of $\delta^{13}C$ of transported sediment fell between the upland and instream source end-members, and $\delta^{13}C$ of transported sediment showed dependence on peak water discharge for the stream during the period when the
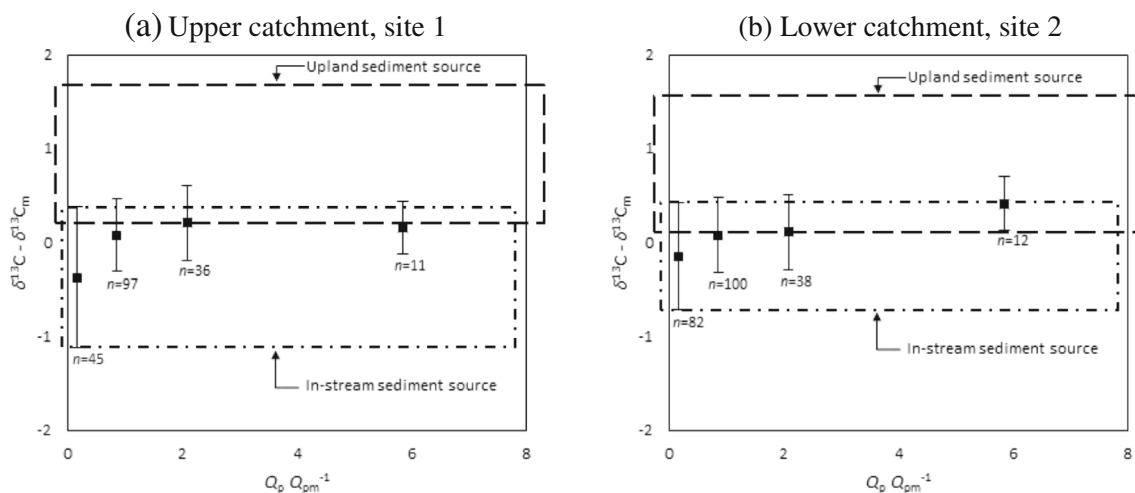

Fig. 5 Stable carbon isotopes of sediment as a function of water discharge at the watershed outlet for the **a** upper catchment and **b** lower catchment sampling location. Source plots are included for the upland sediment and instream sediments. The x-axes plot the hydrograph peak (labeled as Q_p) during which each sediment sample was collected normalized by the mean observed flow rate for all transported sediment data (Q_{pm}). The y-axes plot the stable carbon isotope value of sediments after subtracting the mean. n represents the number of samples collected for each flow regime

sediment trap collected the sediment (see Fig. 5). We normalized the hydrologic events presented on the *x*-axis in Figs. 5 and 6 by dividing the observed peak flow rate (Q_p) by the mean flow rate (Q_{pm}) observed while collecting all of the sediment samples. We validated the relation of bulk instream flow intensity parameters to sediment transport by separating streamflow into baseflow and runoff using hydrograph separation techniques (e.g., Hooghoudt 1940; Arnold et al. 1995; Arnold and Allen 1999; Neitsch et al. 2002). Hydrograph separation results showed a consistent increase in the volume of upland runoff produced during hydrologic events of increasing magnitude (see Electronic supplementary material IV, Fig. S1). The results suggested the increased runoff and peak flow produced a greater contribution of upland sediments to the total load, which is reflected in the increased δ^{13}C signatures observed in Figs. 5 and 6. The hydrograph separation results suggest Figs. 5 and 6 capture the nature of

upland runoff and sediment entering the stream network relatively well. However, we recognize one improvement to this work would be quantitative hydrograph separation, as such represented in the research of Gourdin et al. (2015), to validate and better couple water and sediment sources in the instream model. The stable carbon isotope data suggested a dominance of streambed sediment origin during smaller hydrologic events and an increasing contribution of upland sediment as the magnitude of peak discharge increases. The δ^{13}C value of transported sediment was significantly dependent on peak water discharge during an event at both sites (*p* value < 0.001 for the regression slope). However, the results in Fig. 5 suggest even during the most extreme events the contribution of upland and instream sediment sources is on the same order of magnitude. The results generally agree with our previous work in the watershed. We have found substantial loading of upland sediments occurs only during moderate to extreme

(a) Upper catchment, site 1   (b) Lower catchment, site 2
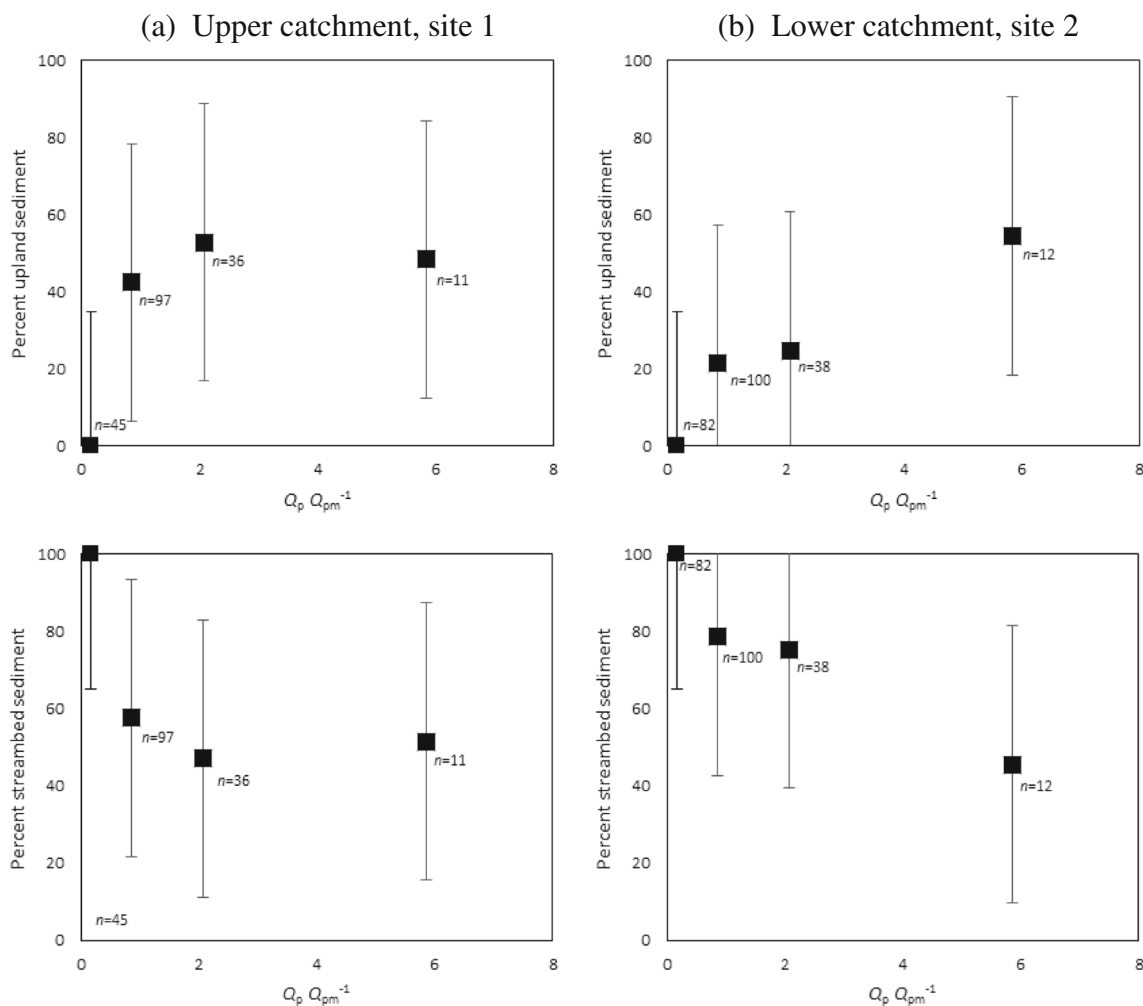
Fig. 6 Sediment fingerprinting results as a function of water discharge for the **a** upper catchment and **b** lower catchment sampling location. The *x*-axes plot the hydrograph peak (labeled as Q_p) during which each sediment sample was collected normalized by the mean observed flow rate for all transported sediment data (Q_{pm}). The *y*-axes plot the percent of upland or streambed contribution, as determined by the sediment fingerprinting results. *n* represents the number of samples collected for each flow regime
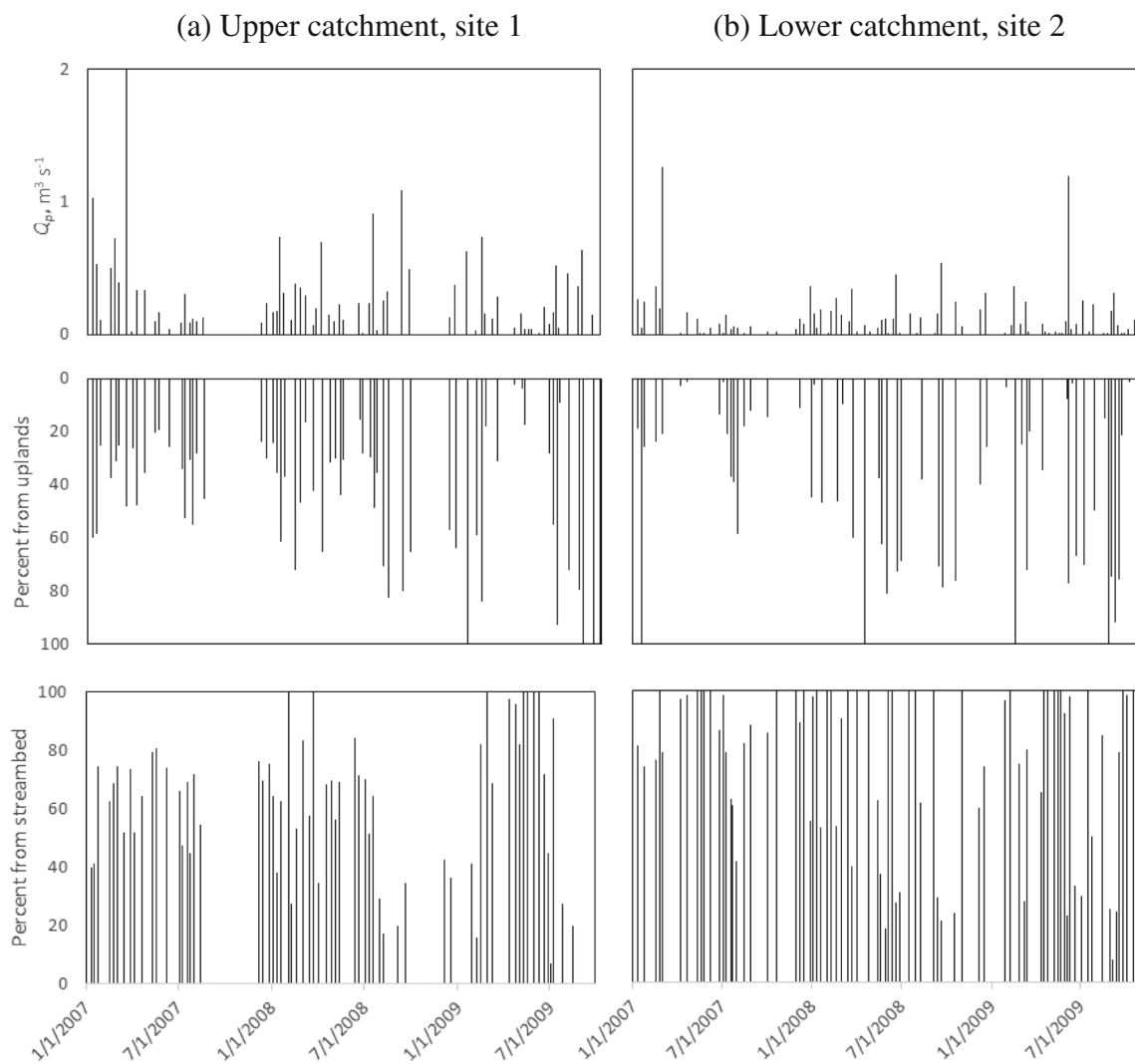
Fig. 7 Source contributions for each event where transported sediments were collected in the **a** upper catchment and **b** lower catchment sampling locations. Q_p is the hydrograph peak ($m^3 s^{-1}$) simulated over the 4-year study period

rainfall events for the gently rolling system (Mahoney et al. 2018). Also, the importance of temporarily stored bed sediments has been suggested across all flow regimes (Russo and Fox 2012). These results agree well with other researchers (e.g., Dalzell et al. 2007; Walling 2005; Fox and Papanicolaou 2007; McCarney-Castle et al. 2017) who also found a significant contribution of distal sediments to total sediment loadings during moderate and high events. For example, Dalzell et al. (2007) used stable carbon isotopes to show a prominence of terrestrial organic carbon in overall organic carbon export during high magnitude hydrologic events. Fox and Papanicolaou (2007) predicted nearly 60% of the eroded soil contributing to the total suspended sediment load during a moderate hydrologic event had upland (proximal) origins.

We carried out the sediment fingerprinting analyses with the stable carbon isotope tracer while accounting for changes in organic matter content of the sources in transported sediments. On average, the upper catchment showed nearly equal percent of sediment originating from the uplands and streambed (see Fig. 6). The lower catchment only showed equal contribution from both upland and instream sources during the 12 most extreme events over the years where we collected samples. For the other hydrologic events, the lower catchment was dominated by approximately three-fourths streambed sediments and one-fourth upland-derived sediments. One main reason attributed to differences in source percentages in the upper and lower catchments is the relative supply of sediment sources. The surface area supplying upland sediment approximately doubles from the upper catchment to lower catchment. However, the surface area supplying streambed sediments is approximately four times greater in the lower catchment compared to the upper catchment.
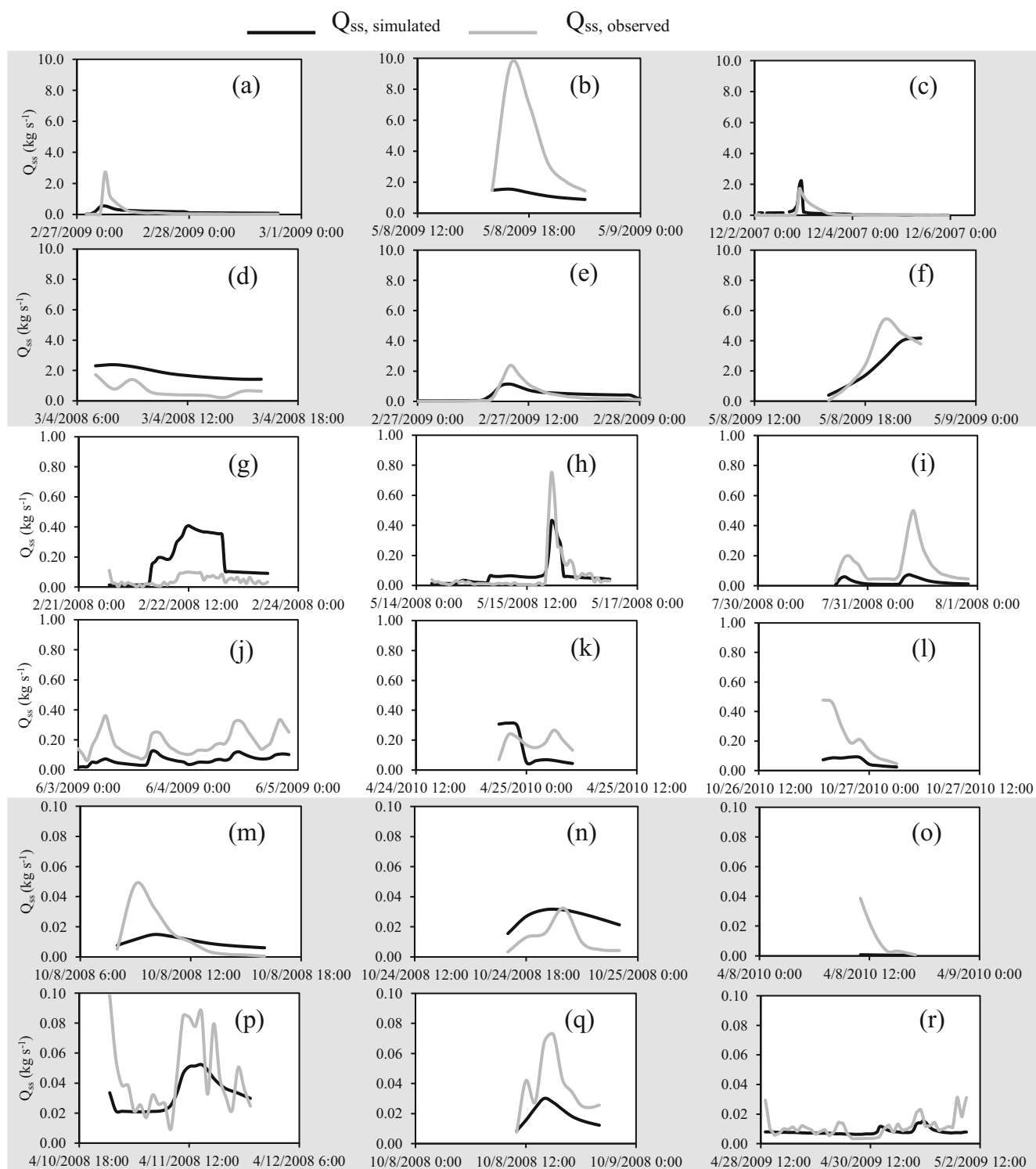
Fig. 8 Simulated Q_{ss} compared with observed Q_{ss}. Model comparison for site 1 (**a**, **b**, **m–o**) and site 2 (**c–l**, **p–r**). Datasets (**a–f**) show events with maximum Q_{ss} of 10 kg s^{-1}. Datasets (**g–l**) show events with maximum Q_{ss} of 1 kg s^{-1}. Datasets (**m–r**) show events with maximum Q_{ss} of 0.1 kg s^{-1}. Three datasets from 2010 (**k**, **l**, **o**) are used for model validation

Uncertainty bounds on the source contributions are high for the sediment fingerprinting results (see Fig. 6), with standard error on the order of 35%, and several reasons explain the high uncertainty. First, we were very conservative in our estimates of uncertainty surrounding $\delta^{13}C$ of sediment sources. We used the standard error of $\delta^{13}C$ surrounding source data to define uncertainty bounds; however, the watershed system averages sources distributions to some degree during erosion and

Fig. 9 Sediment source partitioning during the four flow regimes in the **a** upper and **b** lower catchment. Partitioning results are for scenarios with no simulated equilibrium exchange (i.e., equilibrium exchange equal to zero) and with the calibrated equilibrium exchange. Sediment fingerprinting results aided in the calibration of the exchange factor and are included in the plots. Sediment sources include the streambed (shown with solid bars) and uplands (shown with striped bars)
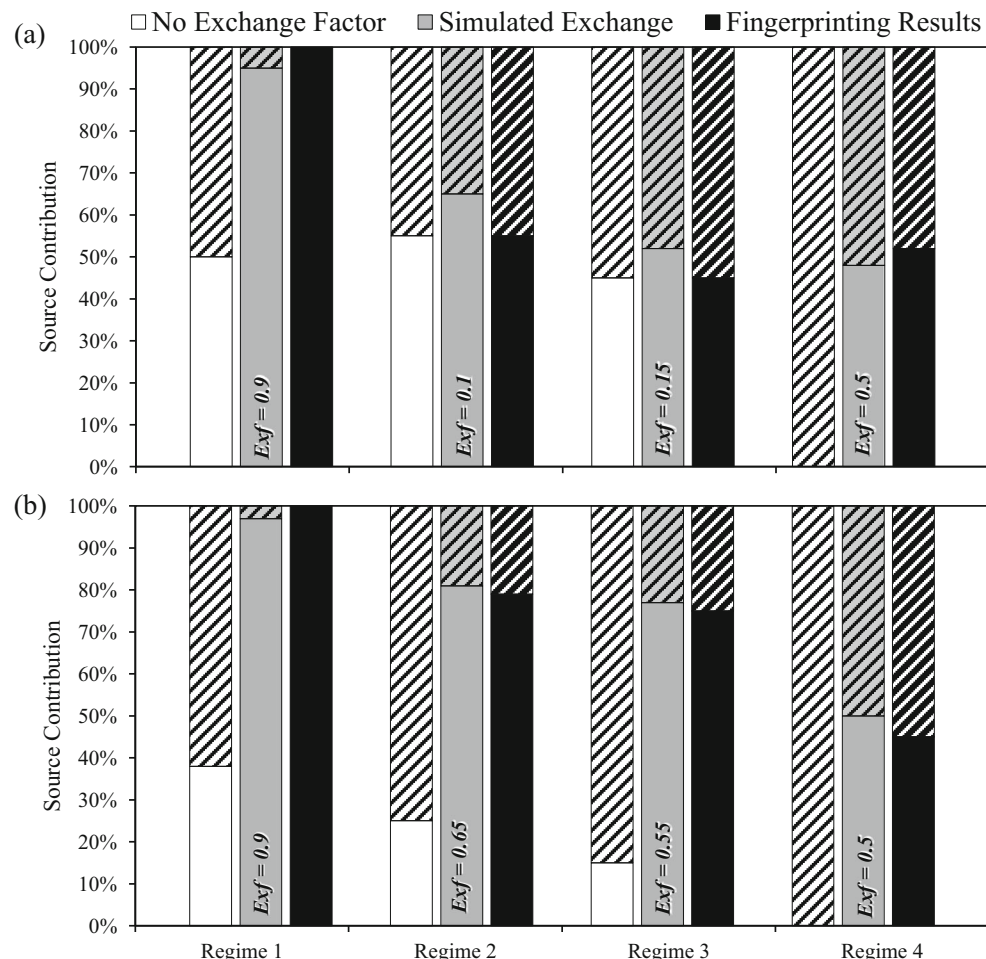
transport (Fox and Papanicolaou 2008a). For example, for moderate and extreme hydrologic events, only 4 out of 294 data (1.3%) of transported sediment $\delta^{13}C$ values fell outside the $\delta^{13}C$ source distribution space defined in Fig. 5. Second, uncertainty in the results of Fig. 6 reflects temporal variability in episodic sediment transport for the 294 hydrologic events samples, as opposed to the uncertainty associated with the tracer error in sediment fingerprinting modeling. Episodic variability exists as a spatially explicit sediment source may be pronounced due to rainfall variability or disturbances. The temporal variability of individual hydrologic events is reflected in Fig. 7. Similar to Fig. 6, the event results show the upland contribution is higher during larger hydrologic events, the streambed is a greater contributor overall, and the streambed is a greater contributor of sediment in the lower catchment relative to the upper catchment. At the same time, the event-to-event variability of upland versus streambed contributions is sometimes substantial in the results of Fig. 7, even when inspecting results from nearly equal peak flow conditions. Results highlight the episodic variability of sediment transport in the basin when considering many hydrologic events. In summary, the mean source contributions in Fig. 6

capture temporal variability of processes and are very conservative concerning error placed on tracer error at the source. Therefore, we have more confidence in the mean values then perhaps reflected by the error bars because they represent variability of hydrologic events as opposed to error introduced from sampling and analyses.

As one discussion point, the reader is reminded of the nonstationary assumption of the streambed sediment source, which is differentiated from the term "nonconservative" where the former reflects the changing tracer signature of the source at the source while the latter reflects the changing of the tracer signature during transport from source to sink. The biology of the streambed continuously evolves due to physical and biogeochemical processes, and in turn, the organic tracer fingerprint was nonstationary (Fox et al. 2010; Fox and Martin 2015). We needed to subtract the nonstationary mean $\delta^{13}C$ using the empirical mode decomposition results of Ford et al. (2015a). Our application and results herein are in the context of previous studies where the nonstationary signature of stable carbon and nitrogen isotopes should be considered during sediment fingerprinting. Fox et al. (2010) used numerical modeling of the stable nitrogen isotopes of
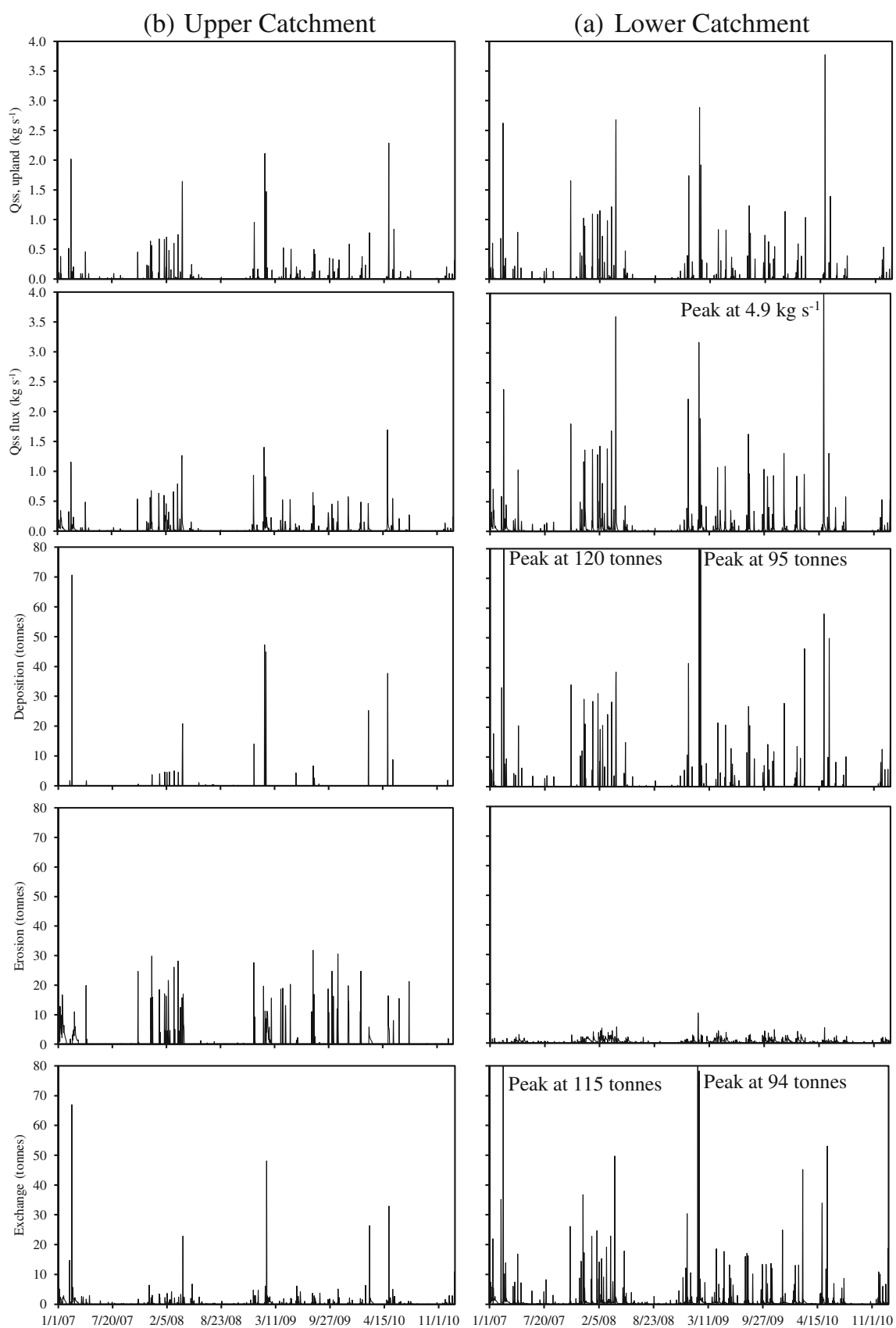
Fig. 10 Upland erosion and sediment transport outputs from 2007 to 2010 for the **a** upper catchment and **b** lower catchment. Model results include upland erosion rate ($Q_{ss,\ upland}$), sediment flux (Q_{ss} flux), instream deposition, instream erosion, and instream equilibrium sediment exchange. For scaling purposes, Q_{ss} plots from 0.0 to 4.0 kg s^{-1} and deposition, erosion, and exchange plots from 0 to 80 t. Peaks greater than the shown range are labeled

Table 2 Upland erosion model inputs and parameters

Parameter	Description	Value/parameter range	Units
A_1	Contributing area, bin 1	116	m^2
A_2	Contributing area, bin 2	951	m^2
A_3	Contributing area, bin 3	34,079	m^2
$\tau_{cr,\ upland}$	Upland critical shear stress	0.10–10	Pa
S_1	Longitudinal slope, bin 1	0.16	$m\ m^{-1}$
S_2	Longitudinal slope, bin 2	0.13	$m\ m^{-1}$
S_3	Longitudinal slope, bin 3	0.12	$m\ m^{-1}$
w_1	Channel width, bin 1	0.08	m
w_2	Channel width, bin 2	0.12	m
w_3	Channel width, bin 3	0.44	m
ε/D	Upland relative roughness	0.00001–1	Unitless
ρ_d	Bulk density of eroded sediment	1400	$kg\ m^{-3}$
t_1	Storm length, erosion time bin 1	0.017–0.167	h
t_2	Storm length, erosion time bin 2	0.183–0.367	h
t_3	Storm length, erosion time bin 3	0.383–0.667	h
k_d	Erodibility coefficient	1.0×10^{-10}–1.0×10^{-8}	$cm^3\ N^{-1}\ s^{-1}$
L_1	Channel length, bin 1	Varies daily	m
L_2	Channel length, bin 2	Varies daily	m
L_3	Channel length, bin 3	Varies daily	m
ρ_w	Density of fluid	1000	$kg\ m^{-3}$

benthic sediments to show seasonality of the tracer in the context of sediment fingerprinting. Fox and Martin (2015) showed the stable carbon and nitrogen fingerprint of sediment from forest sediments exhibited nonstationarity in a 2-year period following drastic forest disturbance from ice storms and tree tip-over. Results highlight that a nonstationary tracer signature of the streambed sediment source needs to be considered when stable isotopes are used in sediment fingerprinting.

5.2 Numerical modeling of the equilibrium sediment exchange

Calibration and validation of the coupled upland and instream sediment transport model showed, in general, the model captured well both sediment leaving the upper catchment and lower catchment (see Fig. 8). Optimum parameters from model calibration are reported in Table 4. The Nash Sutcliff parameter of the model solution space was 0.37, which shows acceptable performance of the model (Moriasi et al. 2007). Sediment yield from the watershed was 2180 ± 330 t km^{-2} $year^{-1}$, which was similar to previous estimates for the basin (Russo and Fox 2012; Mahoney et al. 2018). Global sensitivity analysis of the coupled model showed the erodibility coefficient in the upland model was the most sensitive parameter to sediment flux from the outlet followed by the instream sediment transport carrying capacity of the flow. The erodibility coefficient directly impacts the fluvial erosion rate in upland gullies, swales, and ditches, while the transport

capacity estimate dictates when a model reach will erode or deposit sediment in a given time step. The sensitivity highlights the importance of both upland and instream processes to sediment transport prediction.

The contribution of sediment originating from upland sediments and streambed sediments was sensitive to the equilibrium sediment exchange process, and we found a significant improvement in model results when including the equilibrium exchange process versus model runs when the equilibrium exchange was excluded (see Fig. 9). Inclusion of the equilibrium exchange was needed to replicate results of the sediment fingerprinting. In this manner, the sediment fingerprinting results provided independent information to assist with investigating sediment transport.

As a discussion point, the efficacy of the sediment fingerprinting results to constrain the sediment exchange process provides an example of an emerging class of sediment transport studies coupling sediment fingerprinting and sediment transport modeling. Sediment fingerprinting and sediment transport modeling have advanced in parallel in recent years. Sediment fingerprinting has progressed from a research tool to an accepted method with usefulness in watershed management applications (Mukundan et al. 2012). Sediment transport models have been developed for various applications the past three decades with off-the-shelf tools available to the modeler and various sediment processes considered (Papanicolaou et al. 2008). While these advancements have been in parallel, they have also been somewhat independent, and it appears the time is ripe for greater coupling of these tools. For example,

Table 3 Instream sediment transport model inputs and parameters

Parameter	Description	Value/parameter range	Units
ρ_w	Density of fluid	1000	kg m^{-3}
ρ_{bank}	Density of bank sediment	1500	kg m^{-3}
ρ_{SFGL}	Density of SFGL sediment	1000	kg m^{-3}
$C_{\tau(2)}$	Shear stress coefficient for unsteady flow	1–100	Unitless
$C_{tc(low)}$	Transport capacity coefficient for low flows	6.0×10^{-7}–1.5×10^{-6}	m$^{1/2}$ s^2 kg$^{-1/2}$
$C_{tc(high)}$	Transport capacity coefficient for high flows	6.0×10^{-7}–1.5×10^{-6}	m$^{1/2}$ s^2 kg$^{-1/2}$
ω_s	Mean settling velocity of suspended material	0.00036–0.00240	m s^{-1}
κ	Von Karmen coefficient	0.4	Unitless
$D_{SFGL,\ max}$	Maximum depth of SFGL	0.001–0.010	m
t_d	Development time of the SFGL layer	300–3000	s
$G_{SFGL,Bio}$	Generation rate of SFGL biofilm	1.81×10^{-9}	kg m^{-2} s^{-1}
$\tau_{cr(sfgl)}$	Critical shear of the SFGL source	0.024–1.20	Pa
$\tau_{cr(bed)}$	Critical shear of the bed source	1.0–10.0	Pa
$\tau_{cr(bank)}$	Critical shear of the bank source	10.0–93.0	Pa
$a_{(sfgl)}$	Erodibility of the SFGL source	1.0×10^{-4}–1.0×10^{-2}	kg Pa^{-1} m^{-2} s^{-1}
$a_{(bed)}$	Erodibility of the bed source	1.0×10^{-5}–1.0×10^{-3}	kg Pa^{-1} m^{-2} s^{-1}
$a_{(bank)}$	Erodibility of bank source	1.0×10^{-6}–2.0×10^{-4}	kg Pa^{-1} m^{-2} s^{-1}
k_{ss}	Sediment routing coefficient	0.00–0.50	Unitless
k_s	Flood wave coefficient	0.0	Unitless
N_{reach}	Number of reaches in the stream segment	2	Unitless
	Bank sideslope	16.858	°
B_{upper}	Channel bottom width, upper catchment	6	m
B_{lower}	Channel bottom width, lower catchment	11	m
n_{upper}	Manning's coefficient, upper catchment	0.03	Unitless
n_{lower}	Manning's coefficient, lower catchment	0.03	Unitless
S_{upper}	Channel slope, upper catchment	0.0009	m m^{-1}
S_{lower}	Channel slope, lower catchment	0.00044	m m^{-1}
$L_{reach,\ upper}$	Channel length, upper catchment	18	m
$L_{reach,\ lower}$	Channel length, lower catchment	10	m
$H_{bank,\ upper}$	Bankfull depth, upper catchment	2	m
$H_{bank,\ lower}$	Bankfull depth, lower catchment	2	m
$Q_{boundary,\ upper}$	Boundary flow, upper catchment	1	m^3 s^{-1}
$Q_{boundary,\ lower}$	Boundary flow, upper catchment	2	m^3 s^{-1}
K_p	Settling depth coefficient	0.10–1.0	Unitless
$Exf_{Upper,\ Regime\ 1}$	Upper catchment exchange factor, flow regime 1	0.0–1.0	Unitless
$Exf_{Upper,\ Regime\ 2}$	Upper catchment exchange factor, flow regime 2	0.0–1.0	Unitless
$Exf_{Upper,\ Regime\ 3}$	Upper catchment exchange factor, flow regime 3	0.0–1.0	Unitless
$Exf_{Upper,\ Regime\ 4}$	Upper catchment exchange factor, flow regime 4	0.0–1.0	Unitless
$Exf_{Lower,\ Regime\ 1}$	Lower catchment exchange factor, flow regime 1	0.0–1.0	Unitless
$Exf_{Lower,\ Regime\ 2}$	Lower catchment exchange factor, flow regime 2	0.0–1.0	Unitless
$Exf_{Lower,\ Regime\ 3}$	Lower catchment exchange factor, flow regime 3	0.0–1.0	Unitless
$Exf_{Lower,\ Regime\ 4}$	Lower catchment exchange factor, flow regime 4	0.0–1.0	Unitless

most instream sediment transport models do not account for soil contributions from the uplands (Papanicolaou et al. 2008), yet sediment fingerprinting can readily provide this information to the modeler. The example in this study serves as one step toward meeting this goal. Another recent study showed sediment fingerprinting was useful for calibrating watershed sediment transport model parameters, including the transport capacity coefficient, sediment delivery ratio for reclaimed mining soils, and stream bank erosion parameters (Fox and Martin 2015). We suggest the community might welcome

Table 4 Optimum parameter values for upland erosion model and instream connectivity model

Parameter	Optimum value	Units
$C_{tc(low)}$	8.45×10^{-7}	$\mathrm{m}^{1/2}\ \mathrm{s}^2\ \mathrm{kg}^{-1/2}$
$C_{tc(high)}$	7.12×10^{-7}	$\mathrm{m}^{1/2}\ \mathrm{s}^2\ \mathrm{kg}^{-1/2}$
ω_s	0.00079	$\mathrm{m}\ \mathrm{s}^{-1}$
$\tau_{cr(sfgl)}$	0.11	Pa
$\tau_{cr(bed)}$	5.68	Pa
$\tau_{cr(bank)}$	12.69	Pa
$a_{(sfgl)}$	7.54×10^{-4}	$\mathrm{kg}\ \mathrm{Pa}^{-1}\ \mathrm{m}^{-2}\ \mathrm{s}^{-1}$
$a_{(bed)}$	5.84×10^{-5}	$\mathrm{kg}\ \mathrm{Pa}^{-1}\ \mathrm{m}^{-2}\ \mathrm{s}^{-1}$
$a_{(bank)}$	1.64×10^{-4}	$\mathrm{kg}\ \mathrm{Pa}^{-1}\ \mathrm{m}^{-2}\ \mathrm{s}^{-1}$
$C_{\tau(2)}$	16.6	Unitless
k_{ss}	0.24	Unitless
t_d	1122	s
$D_{SFGL,\ max}$	0.002	m
K_p	0.98	Unitless
t_1	0.075	h
t_2	0.235	h
t_3	0.644	h
$\tau_{cr,\ upland}$	4.02	Pa
k_d	6.91×10^{-9}	$\mathrm{cm}^3\ \mathrm{N}^{-1}\ \mathrm{s}^{-1}$
ε/D	0.74	Unitless
$Exf_{Upper,\ Regime\ 1}$	0.90	Unitless
$Exf_{Upper,\ Regime\ 2}$	0.10	Unitless
$Exf_{Upper,\ Regime\ 3}$	0.15	Unitless
$Exf_{Upper,\ Regime\ 4}$	0.50	Unitless
$Exf_{Lower,\ Regime\ 1}$	0.90	Unitless
$Exf_{Lower,\ Regime\ 2}$	0.65	Unitless
$Exf_{Lower,\ Regime\ 3}$	0.55	Unitless
$Exf_{Lower,\ Regime\ 4}$	0.50	Unitless

additional studies under this theme as we expect many different permutations of the modeling and fingerprinting coupling are possible.

Sediment transport results show the equilibrium exchange process transfers sediment on the same order of magnitude as erosion and deposition fluxes in both the upper and lower catchments over the 4-year simulation period (see Figs. 10 and 11). The results illustrate the process as significant. Calibration of the equilibrium process was data-driven via the fingerprinting results (see Fig. 9). However, some comparison of the results and consideration of the parameters in Eqs. (1) and (2) is worthwhile. The empirically fit exchange factor decreased in value as the peak discharge of the hydrologic event increased for the first three flow regimes, but then increased in value for the fourth flow regime for the upper catchment (Fig. 9, Table 4). The first three flow regimes, in general, could be classified as net streambed erosion events, while the most extreme events of the fourth flow regime

deposited high amounts of sediment to the streambed, i.e., net deposition events in the upper catchment. The exchange factor decreased in value as the peak discharge of the hydrologic event increased for all four events in the lower catchment (Fig. 9, Table 4). One explanation for the inverse relationship between the exchange coefficient and discharge during erosion events is an increase in the bursting period and a smaller contribution of the overall flow depth experiencing exchange. The bursting period is proportional to the flow depth (Nezu and Nakagawa 1993), and the flow depth would be inversely related to exchange in Eq. (2). We might also expect a smaller proportion of suspended particles to be impacted by bursting as the flow depth increases, albeit the connectivity of macroturbulence to near-bed bursting adds uncertainty to this process (Stewart and Fox 2015). During the most extreme events of the fourth flow regime, deposition of suspended sediment from the uplands to the streambed dominates transport in the stream. The extreme events have been found to cause a net increase in streambed storage (Ford et al. 2015b). However, our fingerprinting results suggest the extreme events also have a pronounced contribution of streambed sediment, and the equilibrium exchange coefficient reflected the process.

Several other factors in Eqs. (1) and (2) are also worthy of discussion. Bed sediment availability is directly accounted for when including the surface area of the streambed sediments in the lower and upper catchments, although we assume similarity of particle size distributions during exchange. The assumption is justified based on the highly similar estimates of particle size parameters across flow regimes and over time for the study stream (Fox et al. 2014), which suggests a similar particle size distribution regardless of the source distributions or extent of exchange. We suggest shear threshold also has little impact on bed sediment availability in this study, given the presence of the loosely held and near buoyant surficial fine-grained laminae across much of the streambed (Russo and Fox 2012; Mahoney 2017). While we marginalize these impacts in our system, other watersheds may show dependence of equilibrium exchange on particle size distribution changes and shear thresholds.

The duration of the process in Eq. (2) is particularly noteworthy for discussion. The duration of the equilibrium exchange process reflects the sediment transport time step in model simulation. Erosion and deposition were mutually exclusive in a model time step, and therefore, we might expect the exchange coefficient to decrease as the model resolution is increased. The coefficient is therefore expected to be dependent on model resolution. One surmised numerical modeling attempt to account for the equilibrium sediment exchange processes would be to simulate sediment transport at the time scale of turbulent bursting when the exchange process is occurring. However, this subsecond/centimeter-scale coherent process controlling fluid momentum and sediment exchange

Fig. 11 Sediment budget including the equilibrium sediment exchange for the **a** upper catchment and **b** lower catchment over the simulation period (2007–2010)

(b) Upper catchment sediment budget

Upland Erosion
2820 tonnes

SFGL, Bed,
Bank Erosion
1250 tonnes

Instream Deposition
347 tonnes

Equilibrium
Exchange
621 tonnes

Suspended Sediment Yield
3730 tonnes

(a) Lower catchment sediment budget

Upper Catchment Yield
3730 tonnes

Upland Erosion
4860 tonnes

SFGL, Bed,
Bank Erosion
685 tonnes

Instream Deposition
1440 tonnes

Equilibrium
Exchange
1930 tonnes

Suspended Sediment Yield
8710 tonnes

directed from and to the streambed can only be resolved using direct numerical simulation (DNS) modeling, which is impractical for watershed sediment transport modeling (Papanicolaou et al. 2008). Additionally, the efficiency of a burst to subsequently fallout and pick up sediment is unknown and requires experimentation. Therefore, physically and explicitly representing the bursting-driven equilibrium sediment exchange in a watershed scale model is not practical at this time. We use data-driven results from sediment fingerprinting to help calibrate the equilibrium sediment exchange simulated in our modeling, and we hope the work here might be built on to develop other semitheoretical approaches.

Finally, equilibrium sediment exchange impacts the quality of sediment in the streambed and sediment transported from the watershed. This concept is reflected in the sediment fingerprinting data and results in Figs. 5 and 6. In this watershed, sediment originating from the uplands is more recalcitrant in nature with lower overall carbon content as compared to the labile autochthonous carbon accrued in streambed sediments (Ford and Fox 2017). The evolving streambed and sediment load include a changing matrix of inert and labile sediment carbon as a function of upland and instream processes. To this end, equilibrium sediment exchange should be considered

when the sediment continuum is used to investigate the evolving critical zone.

6 Conclusions

This research provided new coupling of sediment fingerprinting and watershed modeling methods to elucidate the role of the equilibrium sediment exchange process. Our results suggest equilibrium sediment exchange is a substantial process occurring in the system studied. The process does not change the sediment load or streambed sediment storage but does impact the quality of sediment residing in the streambed. Therefore, we suggest equilibrium sediment exchange should be considered when the sediment continuum is used to investigate the critical zone.

Coupling sediment fingerprinting with watershed modeling is a new area of research deserving substantial development. We outline future research priorities for coupling the methods as follows:

1. Improved coupling of sediment fingerprinting time scales with watershed modeling time scales is needed. Sediment fingerprinting results typically have high variance on a

daily basis due to the episodic nature of erosion and the distribution of tracer signatures across a basin. Watershed modeling results are typically specified for daily or subdaily time steps, and results are more representative of the mean behavior of the watershed during the period. Probabilistic approaches might be advanced for better comparisons between the different time scales.

2. Improved sediment tracking and allocation of sediment provenance and sediment history is needed in watershed modeling. For example, the residence time of deposited sediments and their origin before deposition is rarely accounted in fluvial watershed modeling. This lack of information makes a direct comparison of provenance with sediment fingerprinting results cumbersome. Lagrangian methods and better source fractionalization methods coupled with watershed modeling tools might help overcome this limitation.

3. Improved accounting of spatially explicit erosion prone sources is needed in watershed modeling. Sediment fingerprinting relies on field collection of sediments from erosion-prone surfaces identified in the field via erosion scars and deteriorated morphology. These connected sediment transport pathways often are not spatially explicit in watershed modeling, which hinders coupling of the methods. Sediment connectivity theory serves as one method to inform sediment transport models and design sampling regimes for sediment fingerprinting to improve the coupling of the methods. This advancement will require additional research focused on instream connectivity theory given this topic is underdeveloped in the modeling community.

4. Improved development of physically based formulae for source exchange processes, such as equilibrium sediment exchange, is needed. For example, this present research offered potential governing variables controlling equilibrium exchange, but a predictive model of equilibrium exchange has not yet been developed. Modeling formula accounting for source exchange processes both in the uplands and stream corridor will facilitate better coupling with sediment fingerprinting results.

5. Improved nonconservative tracer simulation via watershed modeling is needed to assist with tracer representation in fingerprinting. Watershed modeling efforts can increasingly quantify both physical and biogeochemical changes of sediment properties, and utilization of these subroutines to assist with sediment fingerprinting is expected to be fruitful.

6. Improved optimization strategies for coupling sediment transport modeling and sediment fingerprinting results are needed. For example, if sediment fingerprinting is simultaneously simulated in sediment transport modeling, sediment sources may be better partitioned during modeling. Optimization of sediment fingerprinting and

watershed modeling using iterative feedback loops and multistep calibration methods serve as one approach. Data assimilation methods applied similarly to tracer-transport models of the atmospheric science community serve as another approach.

Publisher's note Springer Nature remains neutral with regard to jurisdictional claims in published maps and institutional affiliations.

References

Ahmadi SH, Amin S, Keshavarzi AR, Mirzamostafa N (2006) Simulating watershed outlet sediment concentration using the ANSWERS model by applying two sediment transport capacity equations. Biosyst Eng 94(4):615–626

Al Aamery N, Fox JF, Snyder M (2016) Evaluation of climate modeling factors impacting the variance of streamflow. J Hydrol 542:125–142

Alberts EE, Nearing MA, Weltz MA, Risse LM, Pierson FB, Zhang XC, Laflen JM, Simanton JR (1995) Chapter 7 soil component. In: Flanagan DC, Nearing MA, USDA (eds) Water erosion and prediction project hillslope profile and watershed model documentation, NSERL Report No. 10. USDA-ARS National Soil Erosion Research Laboratory, West Lafayette, pp 7.1–7.47

Ambroise B (2004) Variable 'active' versus 'contributing' areas or periods: a necessary distinction. Hydrol Process 18(6):1149–1155

Arnold JG, Allen PM (1999) Automated methods for estimating baseflow and ground water recharge from streamflow records. J Am Water Resour Assoc 35(2):411–424

Arnold JG, Allen PM, Muttiah R, Bernhardt G (1995) Automated base flow separation and recession analysis techniques. Ground Water 33(6):1010–1018

Arnold JG, Srinivasan R, Muttiah RS, Williams JR (1998) Large area hydrologic modeling and assessment part I: model development. J Am Water Resour Assoc 34(1):73–89

Bellanger B, Huon S, Velasquez F, Valles V, Girardin C, Mariotti A (2004) Monitoring soil organic carbon erosion with δ13C and δ15N on experimental field plots in the Venezuelan Andes. Catena 58(2):125–150

Blake WH, Ficken KJ, Taylor P, Russell MA, Walling DE (2012) Tracing crop-specific sediment sources in agricultural catchments. Geomorphology 139:322–329

Bonn BA, Rounds SA (2010) Use of stable isotopes of carbon and nitrogen to identify sources of organic matter to bed sediments of the Tualatin River, Oregon (No. 2010-5154). US Geological Survey, USA

Borselli L, Cassi P, Torri D (2008) Prolegomena to sediment and flow connectivity in the landscape: a GIS and field numerical assessment. Catena 75(3):268–277

Bracken LJ, Turnbull L, Wainwright J, Bogaart P (2015) Sediment connectivity: a framework for understanding sediment transfer at multiple scales. Earth Surf Process Landf 40(2):177–188

Cambardella CA, Elliott ET (1992) Particulate soil organic-matter changes across a grassland cultivation sequence. Soil Sci Soc Am J 56: 777–783

Campbell JE, Fox JF, Davis CM, Rowe HD, Thompson N (2009) Carbon and nitrogen isotopic measurements from southern Appalachian soils: assessing soil carbon sequestration under climate and land use variation. J Environ Eng ASCE 135(6):439–448

Cellino M, Lemmin U (2004) Influence of coherent flow structures on the dynamics of suspended sediment transport in open-channel flow. J Hydraul Eng 130(11):1077–1088

Chang HH (1988) Fluvial processes in river engineering. Krieger Publishing Company, Malabar

Collins AL, Walling DE, Leeks GJL (1997) Source type ascription for fluvial suspended sediment based on a quantitative composite fingerprinting technique. Catena 29(1):1–27

Cooper RJ, Pedentchouk N, Hiscock KM, Disdle P, Krueger T, Rawlins BG (2015) Apportioning sources of organic matter in streambed sediments: an integrated molecular and compound-specific stable isotope approach. Sci Total Environ 520:187–197

Dalzell BJ, Filley TR, Harbor JM (2007) The role of hydrology in annual organic carbon loads and terrestrial organic matter export from a midwestern agricultural watershed. Geochim Cosmochim Acta 71(6):1448–1462

Davis C (2008) Sediment fingerprinting using organic matter tracers to study streambank erosion and streambed sediment storage processes in the South Elkhorn watershed. MSc thesis, University of Kentucky, Lexington, USA

Davis CM, Fox JF (2009) Sediment fingerprinting: review of the method and future improvements for allocating sediment non-point source pollution. J Environ Eng ASCE 135(7):490–504

Dou GR (1974) Similarity theory and its application to design of total sediment transport model, vol 14. Research Bulletin of Nanjing Hydraulic Research Institute, Nanjing, pp 127–139

Droppo IG, Amos CL (2001) Structure, stability, and transformation of contaminated lacustrine surface fine-grained laminae. J Sediment Res 71(5):717–726

Droppo IG, Stone M (1994) In-channel surficial fine-grained sediment laminae. Part I: physical characteristics and formational processes. Hydrol Process 8(2):101–111

Ford WI (2011) Particulate organic carbon fate and transport in a lowland, temperate watershed. MSc thesis, University of Kentucky, Lexington, USA

Ford WI (2014) Control of the surficial fine-grained laminae upon stream carbon and nitrogen cycles. PhD dissertation, University of Kentucky, Lexington, USA

Ford WI, Fox JF (2014) Model of particulate organic carbon transport in an agriculturally impacted stream. Hydrol Process 28(3):662–675

Ford WI, Fox JF (2017) Stabilization of benthic algal biomass in a temperate stream draining agroecosystems. Water Res 108:432–443

Ford WI, Fox JF, Pollock E, Rowe H, Chakraborty S (2015a) Testing assumptions for nitrogen transformations in a low gradient agricultural stream. J Hydrol 527:908–922

Ford WI, Fox JF, Rowe H (2015b) Impact of extreme hydrologic disturbance upon the sediment carbon quality in agriculturally-impacted temperate stream. Ecohydrology 8(3):438–449

Fox JF (2006) Fingerprinting using biogeochemical tracers to investigate watershed processes. PhD dissertation, University of Iowa, Iowa City, USA

Fox JF (2009) Identification of sediment sources in forested watersheds with surface coal mining disturbance using carbon and nitrogen isotopes. J Am Water Resour Assoc 45(5):1273–1289

Fox JF, Davis CM, Martin DK (2010) Sediment source assessment in a lowland watershed using nitrogen stable isotopes. J Am Water Resour Assoc 46(6):1192–1204

Fox JF, Ford WI, Strom K, Villarini G, Meehan M (2014) Benthic control upon the morphology of transported fine sediments in a low-gradient stream. Hydrol Process 28(11):3776–3788

Fox JF, Martin DK (2015) Sediment fingerprinting for calibrating a soil erosion and sediment-yield model in mixed land-use watersheds. J Hydrol Eng 20(6):C4014002

Fox JF, Papanicolaou AN (2007) The use of carbon and nitrogen isotopes to study watershed erosion processes. J Am Water Resour Assoc 43(4):1047–1064

Fox JF, Papanicolaou AN (2008a) An un-mixing model to study watershed erosion processes. Adv Water Resour 31(1):96–108

Fox JF, Papanicolaou AN (2008b) Application of the spatial distribution of nitrogen stable isotopes for sediment tracing at the watershed scale. J Hydrol 358(1–2):46–55

Fryirs K (2013) (Dis) connectivity in catchment sediment cascades: a fresh look at the sediment delivery problem. Earth Surf Process Landf 38(1):30–46

Fryirs KA, Brierley GJ, Preston NJ, Kasai M (2007a) Buffers, barriers and blankets: the (dis) connectivity of catchment-scale sediment cascades. Catena 70(1):49–67

Fryirs KA, Brierley GJ, Preston NJ, Spencer J (2007b) Catchment-scale (dis) connectivity in sediment flux in the upper Hunter catchment, New South Wales, Australia. Geomorphology 84(3):297–316

Gellis AC, Hupp CR, Pavich MJ, Landwehr JM, Banks WS, Hubbard BE, Langland MJ, Ritchie JC, Reuter JM (2009) Sources, transport, and storage of sediment at selected sites in the Chesapeake Bay Watershed. U. S. Geological Survey Scientific Investigations Report 2008-5186, 95 p, USA

Gibbs MM (2008) Identifying source soils in contemporary estuarine sediments: a new compound-specific isotope method. Estuar Coasts 31(2):344–359

Gomez B, Trustrum NA, Hicks DM, Rogers KM, Page MJ, Tate KR (2003) Production, storage, and output of particulate organic carbon: Waipaoa River basin, New Zealand. Water Resour Res 39(6). https://doi.org/10.1029/2002WR001619

Gourdin E, Huon S, Evrard O, Ribolzi O, Bariac T, Sengtaheuanghoung O, Ayrault S (2015) Sources and export of particle-borne organic matter during a monsoon flood in a catchment of northern Laos. Biogeosciences 12(4):1073–1089

Gupta RS (2016) Hydrology and hydraulic systems. Waveland Press, Long Grove

Guy BT, Dickenson WT, Sohrabi TM, Rudra RP (2009) Development of an empirical model for calculating sediment-transport capacity in shallow overland flows: model calibration. Biosyst Eng 103(2): 245–255

Hancock GJ, Revill AT (2013) Erosion source discrimination in a rural Australian catchment using compound-specific isotope analysis (CSIA). Hydrol Process 27(6):923–932

Hanson GJ, Simon A (2001) Erodibility of cohesive streambeds in the loess area of the midwestern USA. Hydrol Process 15(1):23–38

Hooghoudt SB (1940) General consideration of the problem of field drainage by parallel drains, ditches, watercourses, and channels. Publ. No.7 in the series Contribution to the knowledge of some physical parameters of the soil (titles translated from Dutch). Bodemkundig Instituut, Groningen

Husic A, Fox JF, Ford WI, Agouridis C, Currens J, Taylor C (2017) Sediment carbon source, fate, and transport in a Fluviokarst watershed (part 2): numerical model development and application. J Hydrol 549:208–219

Jacinthe PA, Lal R, Owens LB (2009) Application of stable isotope analysis to quantify the retention of eroded carbon in grass filters at the North Appalachian experimental watersheds. Geoderma 148(3–4): 405–412

Jarritt NP, Lawrence DSL (2007) Fine sediment delivery and transfer in lowland catchments: modelling suspended sediment concentrations in response to hydrological forcing. Hydrol Process 21(20):2729–2744

Joe S, Kuo FY (2003) Remark on algorithm 659: implementing Sobol's quasirandom sequence generator. ACM Trans Math Softw 29(1): 49–57

Julien PY, Simons DB (1985) Sediment transport capacity of overland flow. Trans ASAE 28(3):755–0762

Jung BJ, Lee HJ, Jeong JJ, Owen J, Kim B, Meusburger K, Alewell C, Gebauer G, Shope C, Park JH (2012) Storm pulses and varying sources of hydrologic carbon export from a mountainous watershed. J Hydrol 440:90–101

Kouhpeima A, Feiznia S, Ahmadi H, Hashemi SA, Zareiee AR (2010) Application of quantitative composite fingerprinting technique to identify the main sediment sources in two small catchments of Iran. Hydrol Earth Syst Sci Discuss 5:6677–6698

KYAPED (2014) Kentucky aerial photography and elevation data program. Available via http://kygeonet.ky.gov/kyfromabove/. Accessed 30 Jan 2018

Laceby JP, Huon S, Onda Y, Vaury V, Evrard O (2016) Do forests represent a long-term source of contaminated particulate matter in the Fukushima Prefecture? J Environ Manag 183:742–753

Laceby JP, Olley J, Pietsch TJ, Sheldon F, Bunn SE (2015) Identifying subsoil sediment sources with carbon and nitrogen stable isotope ratios. Hydrol Process 29(8):1956–1971

Lambert CP, Walling DE (1988) Measurement of channel storage of suspended sediment in a gravel-bed river. Catena 15(1):65–80

Madej MA, Sutherland DG, Lisle TE, Pryor B (2009) Channel responses to varying sediment input: a flume experiment modeled after Redwood Creek, California. Geomorphology 103(4):507–519

Mahoney DT (2017) Sediment transport modelling using dynamic (dis) connectivity prediction for a bedrock controlled catchment. MSc thesis, University of Kentucky, Lexington, USA

Mahoney DT, Fox JF, Al Aamery N (2018) Watershed erosion modeling using the probability of sediment connectivity in a gently rolling system. J Hydrol 561:862–883

McCarney-Castle K, Childress TM, Heaton CR (2017) Sediment source identification and load prediction in a mixed-use Piedmont watershed, South Carolina. J Environ Manag 185:60–69

McConnachie JL, Petticrew EL (2006) Tracing organic matter sources in riverine suspended sediment: implications for fine sediment transfers. Geomorphology 79(1–2):13–26

McCorkle EP, Berhe AA, Hunsaker CT, Johnson DW, McFarlane KJ, Fogel ML, Hart SC (2016) Tracing the source of soil organic matter eroded from temperate forest catchments using carbon and nitrogen isotopes. Chem Geol 445:172–184

McGrain P (1983) The geologic story of Kentucky. Kentucky Geological Survey, University of Kentucky Special Publication 8: Series XI, Lexington

Minella JPG, Merten GH, Clarke RT (2004) Identification of sediment sources in a small rural drainage basin. IAHS Publ XX, IAHS Press, Wallingford, pp 44–51

Moriasi DN, Arnold JG, Van Liew MW, Bingner RL, Harmel RD, Veith TL (2007) Model evaluation guidelines for systematic quantification of accuracy in watershed simulations. T ASABE 50(3):885–900

Mukundan R, Radcliffe DE, Ritchie JC (2011) Channel stability and sediment source assessment in streams draining a Piedmont watershed in Georgia, USA. Hydrol Process 25(8):1243–1253

Mukundan R, Radcliffe DE, Ritchie JC, Risse LM, McKinley RA (2010) Sediment fingerprinting to determine the source of suspended sediment in a southern Piedmont stream. J Environ Qual 39(4):1328–1337

Mukundan R, Walling DE, Gellis AC, Slattery MC, Radcliffe DE (2012) Sediment source fingerprinting: transforming from a research tool to a management tool. J Am Water Resour Assoc 48(6):1241–1257

Nachtergaele J, Poesen J, Sidorchuk A, Torri D (2002) Prediction of concentrated flow width in ephemeral gully channels. Hydrol Process 16(10):1935–1953

Nadelhoffer KF, Fry B (1988) Controls on natural 15N and 13C abundances in forest soil organic matter. Soil Sci Soc Am J 52:1633–1640

Nazari Samani A, Wasson RJ, Malekian A (2011) Application of multiple sediment fingerprinting techniques to determine the sediment source contribution of gully erosion: review and case study from Boushehr province, southwestern Iran. Prog Phys Geogr 35(3):375–391

Neitsch SL, Arnold JG, Kiniry JR, Srinivasan R, Williams JR (2002) Soil and water assessment tool user's manual version 2000. GSWRL Report 202:02-06, Publ. Texas Water Resources Institute. TR-192, College Station, Texas

Neitsch SL, Arnold JG, Kiniry JR, Williams JR (2011) Soil and water assessment tool theoretical documentation version 2009. Texas Water Resources Institute, College Station

Nezu I, Nakagawa H (1993) Turbulence in open channel flows. IAHR/AIRH Monograph. Balkema, Rotterdam, The Netherlands

Nicholls DJ (2001) The source and behaviour of fine sediment deposits in the River Torridge Devon and their implications for salmon spawning. Unpublished PhD thesis, University of Exeter, Exeter, UK

Papanicolaou AN, Elhakeem M, Krallis G, Prakash S, Edinger J (2008) Sediment transport modeling review—current and future developments. J Hydraul Eng 134(1):1–14

Papanicolaou AN, Fox JF, Marshall J (2003) Soil fingerprinting in the Palouse Basin, USA, using stable carbon and nitrogen isotopes. Int J Sediment Res 18(2):278–284

Partheniades E (1965) Erosion and deposition of cohesive soils. J Hydraul Div 91(1):105–139

Phillips JD (2003) Sources of nonlinearity and complexity in geomorphic systems. Prog Phys Geogr 27(1):1–23

Phillips JM, Russell MA, Walling DE (2000) Time-integrated sampling of fluvial suspended sediment: a simple methodology for small catchments. Hydrol Process 14:2589–2602

Rhoton FE, Emmerich WE, DiCarlo DA, McChesney DS, Nearing MA, Ritchie JC (2008) Identification of suspended sediment sources using soil characteristics in a semiarid watershed. Soil Sci Soc Am J 72(4):1102–1112

Rose LA, Karwan DL, Aufdenkampe AK (2018) Sediment fingerprinting suggests differential suspended particulate matter formation and transport processes across hydrologic regimes. J Geophys Res Biogeosci 123:1213–1229

Russell MA, Walling DE, Hodgkinson RA (2001) Suspended sediment sources in two small lowland agricultural catchments in the UK. J Hydrol 252(1–4):1–24

Russo JP (2009) Investigation of surface fine grained laminae, streambed, and streambank processes using a watershed scale hydrologic and sediment transport model. MSc thesis, University of Kentucky, Lexington, USA

Russo JP, Fox JF (2012) The role of the surface fine-grained laminae in a lowland watershed: a model approach. Geomorphology 171–172: 127–138

Saltelli A, Ratto M, Andres T, Campolongo F, Cariboni J, Gatelli D, Saisana M, Tarantola S (2008) Global sensitivity analysis: the primer. Wiley, New York

Sanford LP, Maa JPY (2001) A unified erosion formulation for fine sediments. Mar Geol 179(1–2):9–23

Schindler Wildhaber Y, Liechti R, Alewell C (2012) Organic matter dynamics and stable isotope signature as tracers of the sources of suspended sediment. Biogeosciences 9(6):1985–1996

Simon A, Thomas RE (2002) Processes and forms of an unstable alluvial system with resistant, cohesive streambeds. Earth Surf Process Landf 27(7):699–718

Sims RP, Preston DG, Richardson AJ, Newton JH, Isgrig D, Blevins RL (1968) Soil survey of Fayette county, Kentucky. USDA Soil Conservation Service, U.S. Government Printing Office, Washington DC

Slimane AB, Raclot D, Evrard O, Sanaa M, Lefèvre I, Ahmadi M, Le Bissonnais Y (2013) Fingerprinting sediment sources in the outlet reservoir of a hilly cultivated catchment in Tunisia. J Soils Sediments 13(4):801–815

Smith HG, Blake WH (2014) Sediment fingerprinting in agricultural catchments: a critical re-examination of source discrimination and data corrections. Geomorphology 204:177–191

Stewart HA, Massoudieh A, Gellis A (2015) Sediment source apportionment in Laurel Hill Creek, PA, using Bayesian chemical mass balance and isotope fingerprinting. Hydrol Process 29(11):2545–2560

Stewart RL, Fox JF (2015) Role of macroturbulence to sustain turbulent energy in decelerating flows over a gravel bed. Geomorphology 248:147–160

Stone M, Droppo IG (1994) In-channel surficial fine-grained sediment laminae. Part II: chemical characteristics and implications for contaminant transport in fluvial systems. Hydrol Process 8(2):113–124

USDA Soil Science Division Staff (2017) Soil survey manual. In: Ditzler C, Scheffe K, Monger HC (eds) USDA handbook 18. Government Printing Office, Washington, DC

Walling DE (2005) Tracing suspended sediment sources in catchments and river systems. Sci Total Environ 344(1–3):159–184

Walling DE, Collins AL, Sichingabula HM, Leeks GJL (2001) Integrated assessment of catchment suspended sediment budgets: a Zambian example. Land Degrad Dev 12(5):387–415

Walling DE, Owens PN, Leeks GJ (1999) Fingerprinting suspended sediment sources in the catchment of the River Ouse, Yorkshire, UK. Hydrol Process 13(7):955–975

Walling DE, Woodward JC (1995) Tracing sources of suspended sediment in river basins: a case study of the River Culm, Devon, UK. Mar Freshw Res 46(1):327–336

Walling DE, Woodward JC, Nicholas AP (1993) A multi-parameter approach to fingerprinting suspended-sediment sources. IAHS Publ XX, IAHS Press, Wallingford, pp 329–338

Winterwerp JC, Van Kesteren WG (2004) Introduction to the physics of cohesive sediment dynamics in the marine environment (Vol. 56). Elsevier, The Netherlands

Yan LJ, Yu XX, Lei TW, Zhang QW, Qu LQ (2008) Effects of transport capacity and erodibility on rill erosion processes: a model study using the finite element method. Geoderma 146(1–2):114–120

Zhang Y, Collins AL, McMillan S, Dixon ER, Cancer-Berroya E, Poiret C, Stringfellow A (2017) Fingerprinting source contributions to bed sediment-associated organic matter in the headwater subcatchments of the River Itchen SAC, Hampshire, UK. River Res Appl 33(10):1515–1526